AD-A039 334 NORTHROP CORP DES PLAINES ILL DEFENSE SYSTEMS DEPT F/G 11/1
LOW RF LOSS METAL-CERAMIC BONDS.(U)
NOV 76 R E RUSSELL F33615-75-C-1096
UNCLASSIFIED 094-007564 AFAL-TR-76-104 NL

1 OF 1
AD
A039334

END
DATE
FILMED
6-77

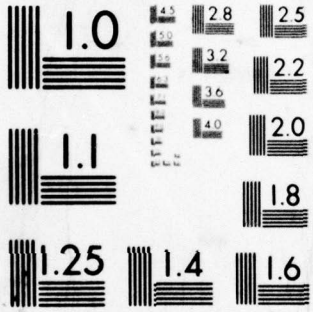

MICROCOPY RESOLUTION TEST CHART
NATIONAL BUREAU OF STANDARDS-1963-A

AD A039334

AFAL-TR-76-104

12

LOW RF LOSS METAL-CERAMIC BONDS

NORTHROP DEFENSE SYSTEMS DEPARTMENT
ELECTRON TUBE SECTION
DES PLAINES, ILLINOIS 60018

NOVEMBER 1976

FINAL TECHNICAL REPORT NOVEMBER 1974 - DECEMBER 1975

APPROVED FOR PUBLIC RELEASE; DISTRIBUTION UNLIMITED

D D C
RECEIVED
MAY 10 1977

NOTICE

When Government drawings, specifications, or other data are used for any purpose other than in connection with a definitely related Government procurement operation, the United States Government thereby incurs no responsibility nor any obligation whatsoever; and the fact that the government may have formulated, furnished, or in any way supplied the said drawings, specifications, or other data, is not to be regarded by implication or otherwise as in any manner licensing the holder or any person or corporation, or conveying any rights or permission to manufacture, use, or sell any patented invention that may in any way be related thereto.

This report has been reviewed by the Information Office (OI) and is releasable to the National Technical Information service (NTIS). At NTIS, it will be available to the general public, including foreign nations.

This technical report has been reviewed and is approved for publication.

John W Bailey

JOHN W. BAILEY, CAPT, USAF
Project Engineer

FOR THE COMMANDER

Donald S. Rees

DONALD S. REES, Acting Chief
Microwave Technology Branch
Electronic Technology Division

Copies of this report should not be returned unless return is required by security considerations, contractual obligations, or notice on a specific document.

AIR FORCE - 20 OCTOBER 75 - 100

UNCLASSIFIED

SECURITY CLASSIFICATION OF THIS PAGE (When Data Entered)

REPORT DOCUMENTATION PAGE

READ INSTRUCTIONS BEFORE COMPLETING FORM

1. REPORT NUMBER: AFAL-TR-76-104

2. GOVT ACCESSION NO.

3. RECIPIENT'S CATALOG NUMBER

4. TITLE (and Subtitle): LOW RF LOSS METAL-CERAMIC BONDS

5. TYPE OF REPORT & PERIOD COVERED: Final Technical Report Period: 11/18/74-12/18/75

6. PERFORMING ORG. REPORT NUMBER: 094-007564

7. AUTHOR(s): Robert E. Russell

8. CONTRACT OR GRANT NUMBER(s): F33615-75-C-1096

9. PERFORMING ORGANIZATION NAME AND ADDRESS
Northrop Defense Systems Department
Electron Tube Section
Des Plaines, Illinois 60018

10. PROGRAM ELEMENT, PROJECT, TASK AREA & WORK UNIT NUMBERS: 2002 02 26

11. CONTROLLING OFFICE NAME AND ADDRESS
Air Force Avionics Laboratory
Air Force Systems Command - U.S. Air Force
Wright-Patterson AFB, Ohio 45433

12. REPORT DATE: November 1976

13. NUMBER OF PAGES: 78

14. MONITORING AGENCY NAME & ADDRESS (if different from Controlling Office)
DCASD Chicago, O'Hare International Airport
P.O. Box 66911
Chicago, Illinois 60666

15. SECURITY CLASS. (of this report): Unclassified

15a. DECLASSIFICATION/DOWNGRADING SCHEDULE

16. DISTRIBUTION STATEMENT (of this Report)

Approved for public release; distribution unlimited.

17. DISTRIBUTION STATEMENT (of the abstract entered in Block 20, if different from Report)

409 984

18. SUPPLEMENTARY NOTES

19. KEY WORDS (Continue on reverse side if necessary and identify by block number)

Sputtered Metallization
Metal-Ceramic Bonds
Thermal Cycling
Titanium Diffusion

20. ABSTRACT (Continue on reverse side if necessary and identify by block number)

This report covers the results of an investigation of a technological process for the production of consistent bonds between metal and ceramic components for use in the rf circuit of high power microwave devices.

Sputter metallization of the ceramic components with the incorporation of a thin active titanium metal layer comprises the basic

→ next page

DD FORM 1 JAN 73 1473 EDITION OF 1 NOV 65 IS OBSOLETE

UNCLASSIFIED

SECURITY CLASSIFICATION OF THIS PAGE (When Data Entered)

process. Special attention was placed on surface smoothness and contamination of the metallization. No heat barrier at the metal-ceramic interfaces was found. Also, low rf losses were realized. The problem of long range failure has been identified as a diffusion phenomenon related to the active metal layer with subsequent formation of a brittle intermetallic which severely limits reliability. Techniques for pinpointing and predicting long term effects and their resultant ramifications have been devised. These techniques have led to an improvement of the sputter metallization process using the Ti-Mo-Cu system, in which these metals are joined by diffusion brazing to a copper meander line.

NTIS
DISTRIBUTION/AVAILABILITY CODES
Dist. AVAIL. and/or SPECIAL
A

TABLE OF CONTENTS

Section		Page
1.	INTRODUCTION	5
2.	ANALYTICAL TOOLS	6
2.1	Pull Test	6
2.2	Peel Test	9
2.3	Microscopy	10
2.4	Scanning Electron Microscope	12
2.5	Ion Microprobe	12
2.6	Electron Microprobe	13
2.7	Mass Spectrometer	13
2.8	Effective Thermal Conductivity	13
2.9	RF Losses	15
3.	MATERIAL	17
3.1	Beryllia Substrate	17
3.1.1	Purity	17
3.1.2	Density	17
3.1.3	Size	17
3.1.4	Surface Roughness	17
3.2	The Hygroscopic Nature of BeO	17
3.3	Surface Contaminants of Virgin Beryllia Substrate	19
3.4	Surface Roughness of the BeO Substrate with Various Preparation Treatments	24
4.	SPUTTERING PROCESS	26
4.1	Background	26
4.2	Apparatus	28
5.	EXPERIMENTAL RESULTS	28
5.1	Hygroscopic Effects of BeO	28
5.2	Copper Sputtered on Beryllia	39
5.3	Molybdenum Plus Copper Sputtered on BeO	39
5.3.1	Metallic Layer Thickness Resolution	39
5.3.2	Sputtered Bond Failure Characteristics	40
5.4	Titanium-Molybdenum-Copper Sputtered on BeO	43

TABLE OF CONTENTS (CONT)

Section		Page
5.4.1	Introduction of an Active Metal Layer	43
5.4.2	Titanium Layer Thickness	44
5.4.3	Effects of Poor Initial Vacuum	44
5.4.4	Residual Stresses	45
5.4.5	Sputter Etching of BeO Substrate	47
5.4.6	Bias Sputtering of Titanium	47
5.4.7	Diffusion of Titanium	48
5.5	Thermal Fatigue	55
5.5.1	Introduction	55
5.5.2	Cycling at 500°C Without Brazing	58
5.5.3	Hygroscopic Effect on Thermal Cycling	58
5.5.4	The Influence of Molybdenum on Thermal Cycling	63
5.5.5	The Influence of Titanium on Thermal Cycling	63
5.5.6	Process Alteration Effects on Thermal Cycling	67
5.5.7	Generalizations	67
5.6	Titanium Diffusion Model	69
6.	CONCLUSIONS	78

LIST OF ILLUSTRATIONS

Figure		Page
1	Pull Test Assembly, Schematic Diagram	7
2	Ductile Fracture in Polycrystalline Metals	8
3	Technique Employed for Peel Test	9
4	Comparison of Sputter Metallization and Moly-Manganese Metallization	11
5	Comparison of Metallizing Layer Thickness	12
6	Statistical Thermal Conductivity Comparison	14
7	Attenuation of Meander Slow-Wave Structure Versus Frequency	16
8	Ion Microprobe Data for Q512 - As Received	20
9	Ion Microprobe Data for Q512 - 500°C Air Fired	21
10	Ion Microprobe Data for Q512 - 1000°C Air Fired	22

LIST OF ILLUSTRATIONS (CONT)

Figure		Page
11	Ion Microprobe Data for Q512 - Sputter Etched	23
12	SEM Photographs of BeO Substrate	25
13	Surface Profile of Beryllia Chip (Q512)	27
14	RF Sputtering Apparatus	29
15	Mass Spectrometer Data (14-Day Delay)	31
16	Mass Spectrometer Data (No Air Firing)	32
17	Failure Tensile Stress Versus Delay After Air Firing	35
18	Film Morphology for Q509	36
19	Film Morphology for Q518	37
20	Film Morphology for Q519	38
21	Copper Distribution for Q530, No Molybdenum	41
22	Copper Distribution for Q527, 2500 Å of Molybdenum	41
23	Tensile Failure Stress Versus Thermal Cycles (Q520)	43
24	Pull Test Assembly After Separation	51
25	Ion Microprobe Data for Coupon Q513 (Chip)	52
26	Ion Microprobe Data for Coupon Q513 (Rod)	53
27	Titanium Diffusion After Thermal Excursions	56
28	Failure Modes With and Without Thermal Cycling	57
29	Deterioration of Bond Strength With Thermal Cycling for Samples With Moisture Entrapment	62
30	Thermal Cycling Effect on Bond Strength for Varying Molybdenum Thicknesses	64
31	Thermal Cycling Effect on Bond Strength for Varying Titanium Thicknesses	65
32	Thermal Cycling Effect on Bond Strength With Minimum Values	66
33	Thermal Cycling Effect on Bond Strength for Different Initial Conditions	68
34	Titanium-Molybdenum Binary Equilibrium Phase Diagram	70
35	Titanium-Copper Binary Equilibrium Phase Diagram	71
36	Titanium Diffusion Schematic for the Ti-Mo-Cu System	72
37	Film Morphology for Q537	75
38	Titanium Spatial Relationships With Thermal Excursions	76
39	Titanium Spatial Relationships for Cycled Chip After Brazing	77

LIST OF TABLES

Table		Page
1	Qualitative Chemical Analysis of Beryllia Chip.	18
2	Tensile Test Data - Delayed Sputtering.	34
3	Tensile Strength Data - Mo Plus Cu Layers	42
4	Camber Measurements of Sputtered Coupons.	46
5	Diffusion Data for Selected Binary Systems.	50
6	Average Counts of Detected Titanium	54
7	Sputtering Process Experimental Variables	59
8	Thermal Cycling Effect on Tensile Strength.	60
9	Thermal Cycling Effect on Sputtered Coupon	61
10	Diffusion Experiments on Coupon Q537.	73

1. INTRODUCTION

One of the most important processes in modern tube technology is the brazing of ceramic and metal parts for the tube envelope and the tube configuration. The brazing process has to fulfill several requirements:

A. Must be vacuum tight

B. Must withstand high temperature changes, ie, support thermal shocks and thermal fatigue

C. Must meet high tolerances

D. Must be of reasonable cost and have some special application, ie, depressed collector rf window or brazed ceramic supports of delay lines

E. Must provide good heat transfer, ie, must not present a thermal barrier for the heat flow

F. Must have low rf losses

Numerous studies on a large number of different brazing processes have been made. The most commonly known and the most reliable process is the moly-manganese process. However, this process is deficient in two main requirements - good heat transfer and low rf losses. The heat transfer between the metal and the ceramic is poor because a thermal barrier is created between the ceramic and the metal by a glassy phase necessary for strong bonding. The rf losses are high because the rf current flows in a film of relatively high resistivity with a roughness that is high compared to the skin depth.

For improvement of the brazing for high power microwave tubes, a study[1] of a process has been made by using the thin film sputtering technique which is currently used in integrated circuit technology. This process lends itself to a smooth surface with no thermal barrier and the use of a high conductivity copper film. As a result, the losses of meander lines in crossed-field amplifiers (cfa) decreased by a factor of 2 from 5 dB to 2.5 dB at 4 GHz and from 10 dB to 5 dB at 8 GHz and approach the theoretical value of a smooth copper line. Moreover, the thermal conductivity approaches the theoretical heat conductivity of the BeO ceramic. No fundamental heat barrier was formed as in

[1] Cook, M.L., Moats, R.R., "Influence of Metal-Ceramic Bonding Process in Cross-Field Amplifier Performance," Conference Record of 1973 Eleventh Conference on Electron Device Techniques, IEEE, New York.

the case of the moly-manganese process. This improvement increased efficiency to 30% (compared to 20% for moly-manganese) and increased average power to more than 1 kW (compared to 750 W for moly-manganese).

However, it was soon found that the new brazing process was much more sensitive to thermal fatigue. The bonding of the sputtered copper line degraded much faster than the moly-manganese line when the temperature was cycled between 500°C and room temperature. The result of this thermal fatigue phenomenon is limited life of the cfa in field operations and low production yields.

The Air Force Avionics Laboratory was aware of this problem and awarded a contract (No. F33615-75-C-1096) to Warnecke to study the thermal fatigue behavior of sputtered metallization. This report describes the findings during the first phase of this program.

2. ANALYTICAL TOOLS

2.1 Pull Test

In order to evaluate the strength of metal-ceramic bonds, a measuring technique must be well defined and economical. The method used consisted of a tensile pull test assembly comprised of a 1/2-inch square portion of a sputtered coupon sandwiched between two OFHC copper rods as depicted in figure 1. This configuration was secured in a stainless steel fixture where a screw, with 20 inch-pounds of torque applied, transmitted pressure to the copper rods during diffusion brazing at 1000°C. Subsequent loading to failure in uniaxial tension was performed. Resultant failure stress measurements provide a direct indication of the adhesion of the composite sputtered films to the beryllia substrate.

The pull test rod assembly also serves as a convenient test vehicle to quantify the effects of thermal cycling. A downward trend of bond strength and changes in the failure mode with thermal cycling were observable.

The rationale in using waffled rods as opposed to solid bars is that given the relatively thin substrate, less shear is imparted to the sputtered surface with the waffled configuration. Since the BeO substrate will not accommodate plastic deformation in tension, the copper rods and the sputtered metallic layers must accommodate all the deformation prior to fracture.

Tensile fracture of moderately ductile polycrystalline metals such as copper eventually produces a necked region as shown in figure 2. Fracture begins at the center of the specimen and then extends by shear along the dashed lines (figure 2). A shear fracture occurs as the result of excessive slip on the active slip planes. This fracture mode is promoted by a resolved shear stress.[2]

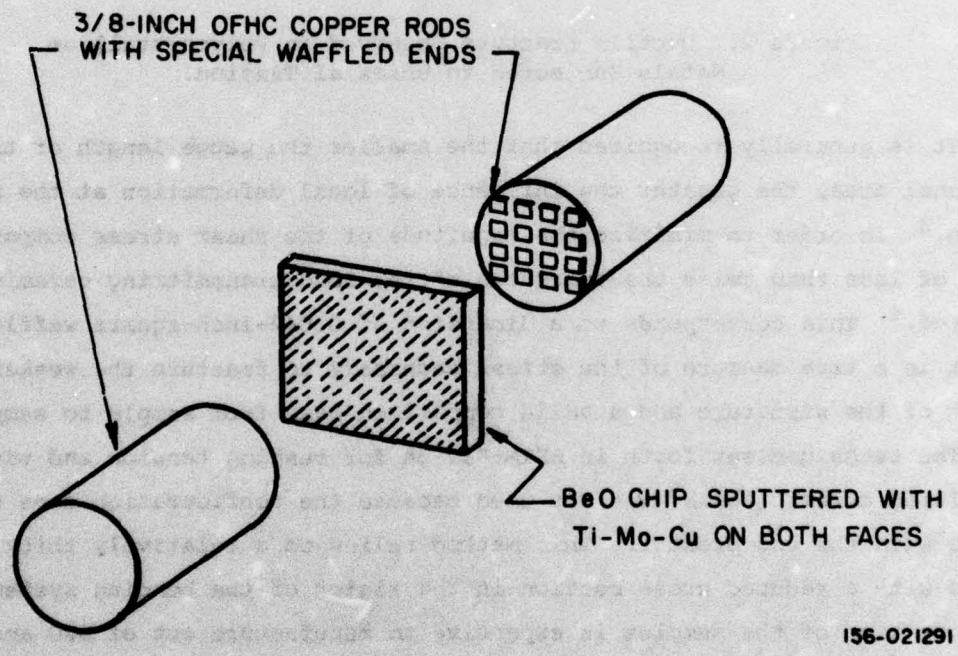

Figure 1. Pull Test Assembly, Schematic Diagram.

[2] Dieter, George E., Mechanical Metallurgy, McGraw-Hill, 1961, p 191.

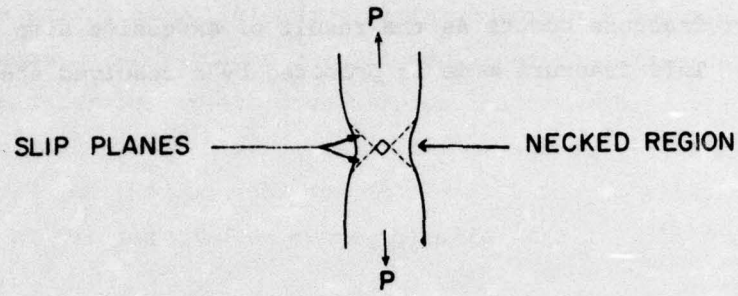

156-021292

Figure 2. Ductile Fracture Observed in Polycrystalline Metals Subjected to Uniaxial Tension.

It is generally recognized that the smaller the gauge length or the cross sectional area, the greater the influence of local deformation at the necked region.[3] In order to minimize the magnitude of the shear stress component, a value of less than twice the thickness of the load transmitting ceramic was selected.[4] This corresponds to a dimension of 0.042-inch-square waffles. The result is a true measure of the stress necessary to fracture the weakest component of the structure and a valid comparison base from sample to sample.

The technique set forth in ASTM-F19-64 for testing tension and vacuum metallized ceramic seals[5] was not used because the configuration does not correlate with the end product. This method relies on a relatively thick ceramic sample with a reduced cross section in the region of the bonding system. The configuration of the samples is expensive to manufacture out of BeO and does not simulate eventual usage. Conventionally, this testing method has been used to evaluate thick film hermetic seals of the moly-manganese type and is not appropriate to the thin-section geometry investigated.

[3] Ibid, p 253.

[4] O'Shea, R., Private Communication to R. Russell, 1975.

[5] American Society for Testing and Materials, "Tension and Vacuum Testing Metallized Ceramics," Specification F19-64, Part 3, p 366-370.

2.2 Peel Test

A technique for evaluating the general adhesion was devised. The test involves scraping the sputtered films with a scalpel blade as depicted in figure 3. Examination under a microscope led to the following rating system:

A. Designates an extremely tenacious film; the copper layer snow plows and will not peel down to the ceramic even after repeated shaving.

B. Designates a fairly strong adhered film; some discontinuous patches of peeled metallizing in a matrix of adherent copper; may require more than one pass of the knife to remove some copper (swiss cheese appearance).

C. Designates a film of moderate strength; peeling occurs continuously with difficulty and only in the area of the knife slice.

D. Designates poor film adherence; peels with little effort in the area of the knife contact region.

E. Designates a film of essentially no adherence; copper peels as a foil with no effort, virtually no knife is needed; lifting can be started and continued with the use of tweezers.

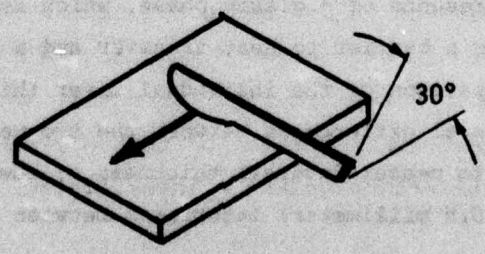

156-021293

Figure 3. Technique Employed for Peel Test.

Rating is subjective, but it reflects a greater level of adherence than the conventional tape test. A tape test similar to TT-P-1757[6] is commonly used, but this test will only discriminate between the lower ratings of D and E designated above. No differentiation can be made between A, B, or C ratings, which are the more critical levels of importance for sputtered films which are intended to positively anchor components to a ceramic substrate. A number of other peel or shear testing methods are in fairly wide use. One test is to braze a strip of Kovar onto the metallized ceramic with a tab left protruding beyond the ceramic edge so that it can be attached to a fixture for pulling and recording the force.[7] This test results in a shear peel failure and is useful where the ceramic is large enough to be easily held. Because of the geometry of thin substrate and the more uniform pull test used for obtaining fracture stresses, the knife peel test is considered to be a discriminating guide to thin film adherence under shear. As a practical quality control test for production usage, it lends itself to quick results, and when coupled with pull test results gives a suitable guide to film integrity.

2.3 Microscopy

Samples of sputtered substrates were mounted perpendicular to the substrate thickness and prepared for conventional metallography. The purpose of this technique is to reveal general film structure and surface irregularities. Figure 4 is a comparison of a thick film moly-manganese metallized substrate versus a thin film sputtered substrate. A marked difference in contour is revealed, the sputtered sample having a very uniform surface compared with the rough surface for the moly-manganese metallized sample. Inherent to the moly-manganese process is the presence of a glassy phase, which is the bonding mechanism. It also acts as a barrier to heat transfer and a source of rf losses. Figure 5 is a comparison of the individual layer thicknesses. Light microscopy reveals the general differences between the two metallizing processes and is a good means to measure overall thicknesses; however, due to the resolution limit of about 0.5 millimeter, interfaces between layers are not discernible.

6 Federal Specification TT-P-1757, "Primer Coating, Zinc Chromate, Low-Moisture-Sensitivity," 14 August 1972.

7 Kohl, Walter H., Handbook of Materials and Techniques for Vacuum Devices, Reinhold Publishing, 1967, p 461.

A. SPUTTER METALLIZING (THIN FILM) X947

B. MOLY-MANGANESE METALLIZING (THICK FILM) X947

156-021294

Figure 4. Comparison of Sputter Metallization and Moly-Manganese Metallization.

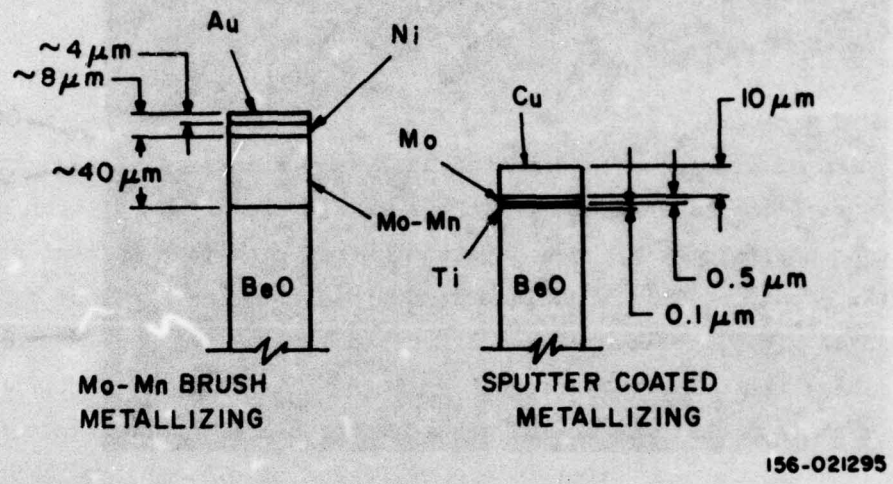

Figure 5. Comparison of Metallizing Layer Thicknesses.

2.4 Scanning Electron Microscope

The advantages of the scanning electron microscope (SEM) arise from the fact that the surface of a sample is available for examination, including simple observation, at resolution much better than that of the optical microscope, and with a depth of field that is orders of magnitude greater. This three-dimensional capability affords an excellent means to study the topology of the ceramic surface and the effects of different preparations prior to metallization.

2.5 Ion Microprobe

To study surface chemistry the ion microprobe is an excellent technique. Oxygen is ionized using a 22-kV potential and directed through a mass spectrum separator; the resultant ions are focused on the sample with a beam diameter of 500 Å. A plasma is established which sputters ions on the surface to a depth of 50 Å. The emitted ions are collected and analyzed using another mass spectrometer.

The output is a relative intensity of a particular emitted ion or a scan of all ions yielding a detailed description of what elements and radicals were

present on the sample surface. By moving the beam across the sample a surface description is obtained. If the beam is left stationary and the ion selection held constant a profile of depth is achieved due to the sputtering into the sample. This analytical technique can be used to study surface contamination, surface chemistry, or concentration gradient of a particular element below the surface.

2.6 Electron Microprobe

If a beam of electrons is directed at a sample surface, X rays are emitted. The X rays can be analyzed for their origin element. By scanning the surface with the incident beam, analysis of X ray renders a spatial mapping of a particular element. This technique lends itself to the study of film morphology and atomic diffusion between sputtered layers.

Typically, the primary electron beam is 50 Å in diameter and penetrates a sample to a nominal depth of 500 Å, depending on the elements involved and the density of the sample. In order to aid selection of elements to be analyzed, an X-ray spectrum is taken of a surface. Detectors are then set for a particular element and a scan taken of the area of interest. This technique was used to examine sputtered film continuity and titanium diffusion after thermal cycling of sputtered products.

2.7 Mass Spectrometer

In the case of the mass spectrometer, gas molecules are bombarded with a beam of energetic electrons. The molecules are ionized and broken into fragments, some of which are positive ions. Each ion has a particular ratio of mass to charge. Ions are analyzed in such a way that a signal is obtained for each mass-to-charge ratio; the signal obtained reflects the relative abundance of each ion.

During sputtering, a mass spectrum was gathered to reveal what gaseous ions are present and how they might be related to the process steps. Only elements which are gases can be analyzed by this method.

2.8 Effective Thermal Conductivity

Given the excellent thermal conductivity of BeO (o_{eff} = 2.5 watts/cm -^{o}C), any metallized layers that are applied which have less effective thermal conductivity pose a heat transfer barrier. A comparison of statistical

thermal conductivity for moly-manganese and sputter metallizing is shown in figure 6. It is evident that the sputter metallizing poses less of a thermal barrier than moly-manganese metallizing.

As a production quality assurance check, assembled meander line configurations are given a thermal test to ascertain if the thermal barrier resistance is sufficiently low to provide adequate heat dissipation. The test involves ac heating of the delay line and taking thermocouple readings at three positions along each line insulator. The resultant temperature readings are referenced to the copper base, giving a thermal gradient. This gradient is

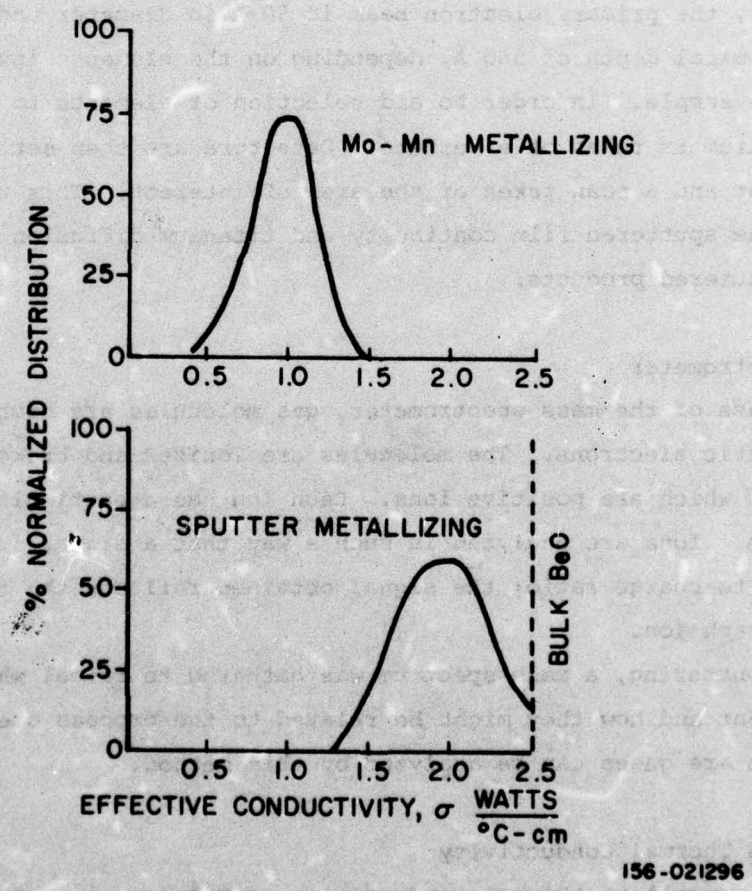

Figure 6. Statistical Thermal Conductivity Comparison.

used to calculate the effective thermal conductivity of the assembly. The significance of this test is in its correlation with tube life related to line failures. In principle, the effective thermal conductivity relates directly to the temperature of the delay line during tube operation. Low thermal conductivity can result in the inability of individual line insulators to conduct away beam-generated heat, causing line melting. The delay line will eventually open up, resulting in a catastrophic failure. This test was not performed for any of the samples in this study as related to metallizing parameters because of its high cost. However, sufficient correlation exists between variables such as tensile strength, thermal cycling and line performance in terms of conductivity that these criteria are relatable. That is, sputtered ceramics that display a low tensile strength exhibit poor thermal conductivity, and after extenced usage run the risk of separation, which yields high thermal resistance.

Therefore, a necessary but not sufficient criterion for thermally related life is bond strength. Bond strength deterioration with thermal cycling is a key indication of thermally induced failures as revealed by thermal testing and tube failures observed in the production of cfa devices.

2.9 RF Losses

In a metal-ceramic bond, the rf current circulates in an outer thin film due to the skin effect. The skin depth is proportional to the square root of resistivity and wavelength; rf losses increase with surface roughness measured relative to the skin depth. For moly-manganese metallizing, the surface of the molybdenum is rough due to the glassy phase between the molybdenum and the ceramic. Also, the resistivity of molybdenum is about three times higher than that of copper. A line brazed by the moly-manganese process will have losses several times higher than those of an ideal copper line with a roughness that is small compared to the skin depth of copper, because of the combined effect of molybdenum itself and the glassy phase that surrounds it. It follows that a loss in efficiency for twt and cfa devices will result from the moly-manganese process. Production delay lines have been constructed using both sputter metallizing and moly-manganese metallizing, and the microwave losses measured by the insertion technique. Figure 7 is a comparison of rf attenuation versus

frequency for both metallizing processes. The measured attenuation compares very well with the mathematical model used to calculate the theoretical attenuation.

The resultant power output observed is 50% greater for sputter metallizing (3 kW) compared to the moly-manganese metallized ceramics (2 kW). Attenuation data has been taken for every delay line structure fabricated and the verification of lower rf power losses or attenuation holds for every sputter metallized product.

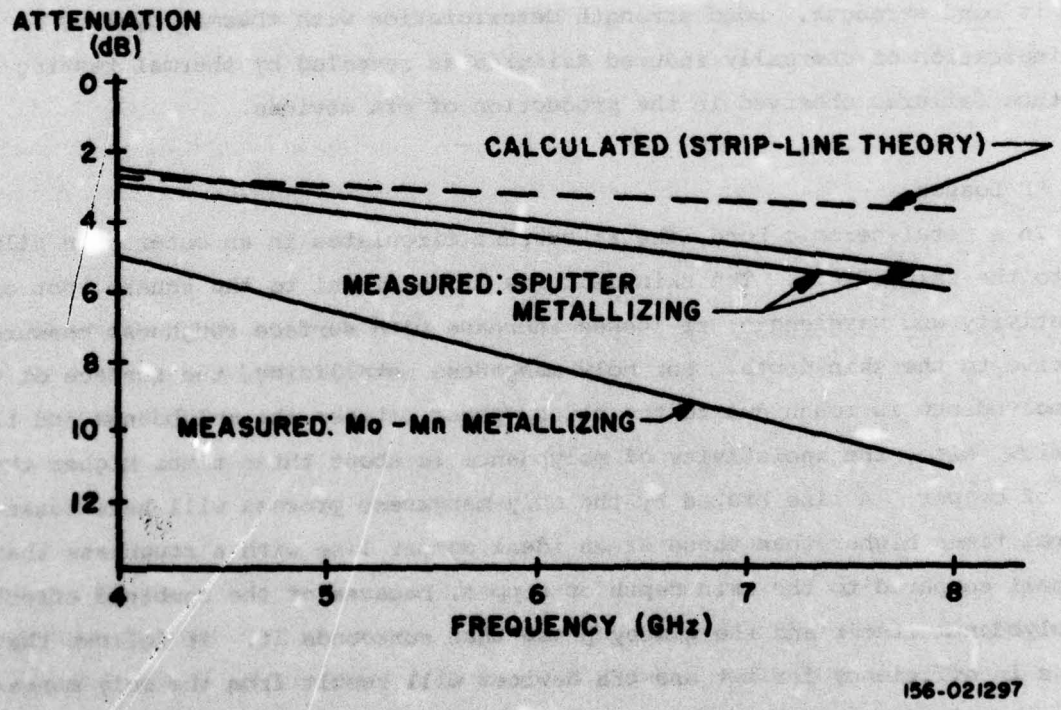

Figure 7. Attenuation of Meander Slow-Wave Structure Versus Frequency.

3. MATERIAL

3.1 Beryllia Substrate

3.1.1 Purity. A bulk chemical analysis of the beryllia substrate material was performed. The results are shown in table 1. The nature of the analysis gives an order of magnitude range and not an exact measure of each constituent present. Based on the analysis, the BeO has a nominal purity of 99.5 weight percent. The additional elements detected are those stated by the manufacturer to be the intentional additives employed in the binder.

3.1.2 Density. Specific gravity of coupon number Q512 was determined to be 2.86 g/cm^3. Nominal specific gravity for commercial BeO products according to the supplier (Accumet Engineering Company) is 2.88 g/cm^3. Maximum theoretical density of BeO is 3.025 g/cm^3. The product used for investigation is 95% of theoretical density.

3.1.3 Size. Substrates used for all work were 2-inch-square coupons. Thickness variation for the coupons was between 0.0214 inch and 0.0217 inch with a maximum tolerance of ± 0.0001 inch for any individual coupon. The camber of each coupon was determined using a go/no-go bridge with a resulting variation of less than 0.0002 inch per inch over the whole 2-inch surface in both directions.

3.1.4 Surface Roughness. The surfaces of the blank coupons were lapped by the supplier and inspected using a profilometer. Measurements were between 5 microinches and 10 microinches, with a variation of no more than ± 2 microinches for any individual coupon.

3.2 The Hygroscopic Nature of BeO

Two virgin coupons were weighed and air fired, one at 500°C and the other at 1,000°C. Immediately after firing, the respective coupons were reweighed, with a weight loss of 0.036% noted for the coupon fired at 500°C and a 0.11% loss noted for the coupon fired at 1,000°C. After 10 days the coupons were weighed once more, and both had regained all the lost weight. The coupons were stored in the open air, covered with glass dishes.

Table 1. Qualitative Chemical Analysis of Beryllia Chip.

Element	Amount (Order of Magnitude Range)
Beryllium	Major
Silicon	0.05 - 0.5
Magnesium	0.01 - 0.1
Copper	0.0005 - 0.005
Iron	0.0005 - 0.005
Aluminum	0.0003 - 0.003
Nickel	0.0003 - 0.003
Silver	0.00001 - 0.0001
Calcium	0.00001 - 0.0001
Tin	Trace 0.001
Molybdenum	Trace 0.001
Lead	Trace 0.001
Sodium	Questionable-if present, 0.05

The formulation of $BeO \cdot XH_2O$ appears to be a critical variable. After sufficient time, moisture will reestablish itself on the BeO substrate. Referring to results obtained during the course of production work, it was observed that a positive correlation existed between the continuity of the metallic layers at the BeO interface and bond strength achieved. The interpretation made was that discontinuous films resulted from entrapped water which was vaporized upon initial sputtering and prevented the first metal deposition from bonding to the substrate. Judging from the results of time lags between air firing and sputtering and the lower bond strengths achieved, and the weight gain of air-fired samples due to the hygroscopic nature of BeO, the generalization regarding water seems to be valid. This makes air firing of coupons immediately prior to sputtering an extremely critical variable.

3.3 Surface Contaminants of Virgin Beryllia Substrates

Ion microprobe analysis was used to ascertain what possible surface contamination might be present on the beryllia substrate prior to sputtering and what effect various treatments may have on them. It is important to bear in mind that the penetration of the ionized beam during analysis is only 50 Å. Coupon Q512 was quartered and the sections were treated as follows: as received (baseline), 500°C air firing, 1,000°C air firing, and sputter etching. The data gathered during ion microprobe scans of each differently treated section are shown in figures 8 through 11. In the as-received condition, high concentration of sodium, magnesium, aluminum, silicon, potassium and calcium are detectable at the surface. All of these elements except potassium are present in the bulk ceramic (table 1). The levels of sodium and potassium are relatively high and their source is not known with absolute certainty. One conjecture is that they may result as residual salts from handling. Also present are various organic moleculars and a hydrated form of beryllium.

After firing at 500°C in air most of the organic moleculars are absent with a marked reduction in most of the binder additives. The exception is that a high level of sodium persists which was not present in the bulk ceramic in any appreciable quantity. After air firing at 1,000°C most of the binder additives increase in concentration at the surface compared to the concentration found in samples fired at 500°C. Aluminum remains low, but sodium, sili-

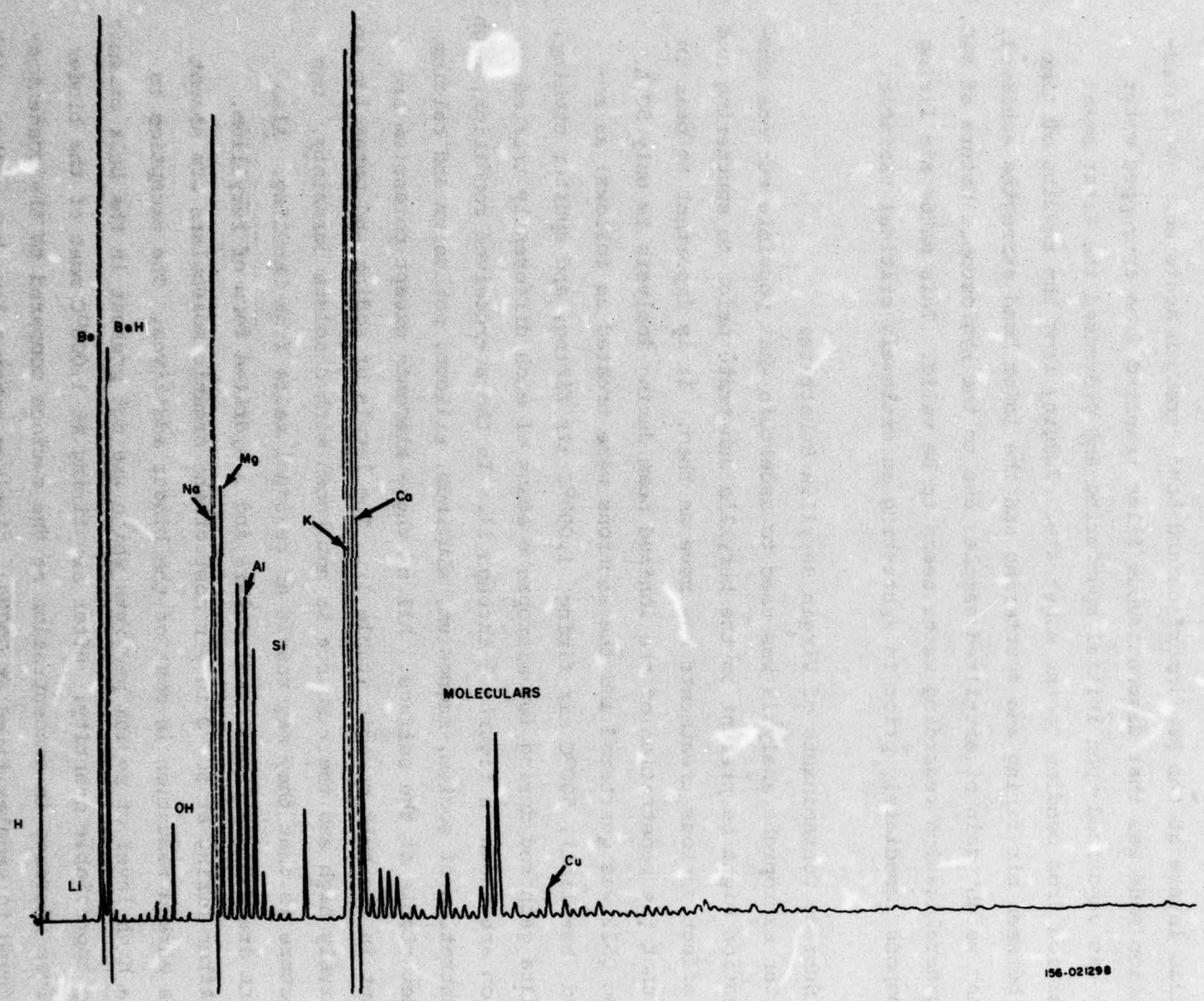

Figure 8. Ion Microprobe Data for Q512 in the As-Received Condition.

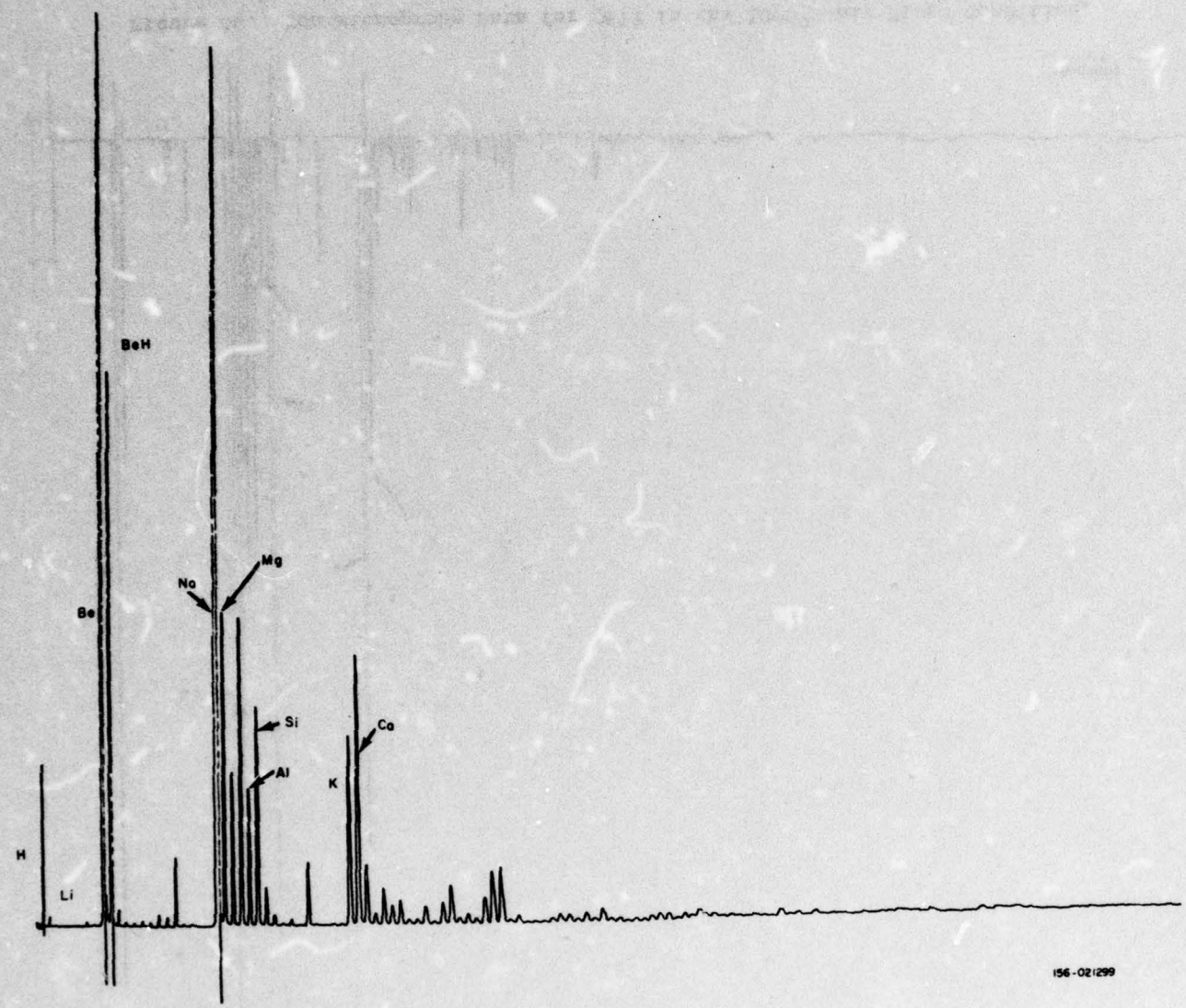

Figure 9. Ion Microprobe Data for Q512 in the 500°C Air Fired Condition.

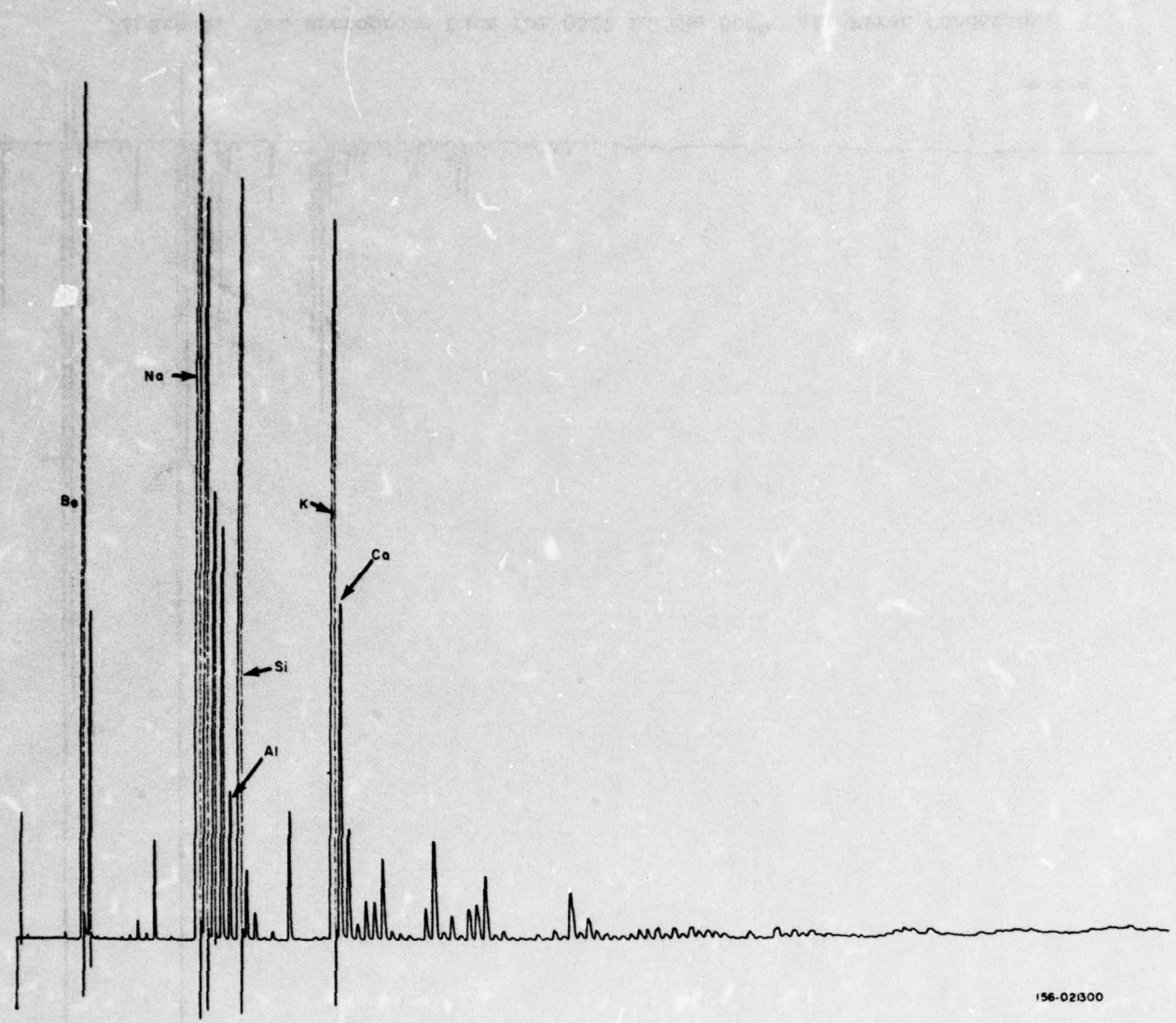

Figure 10. Ion Microprobe Data for Q512 in the 1000°C Air Fired Condition.

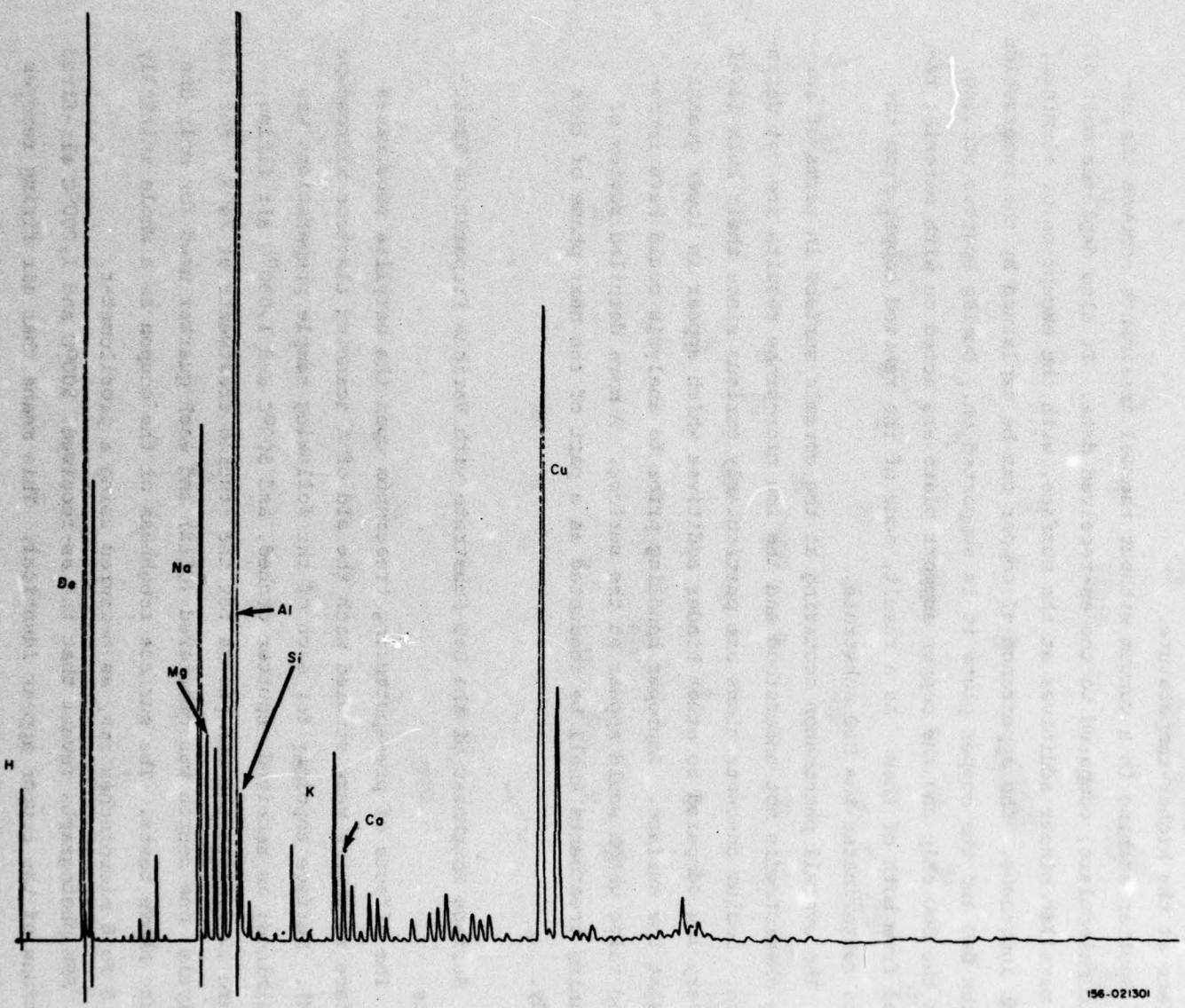

Figure 11. Ion Microprobe Data for Q512 in the Sputter Etched Condition.

con, and magnesium increase to a level higher than that of the as-received state, while potassium and calcium increase only slightly. The increase of all the elements noted is believed to be a result of their migration to the surface at the higher temperature.

Sputter etching in a vacuum without thermal treatments removes the organic moleculars, compared to the as-received data. It also depletes most of the metallic binder additives at the surface, with the exception of aluminum, which increases. The appearance of copper can be explained by the interaction of the BeO and the copper plate it is supported on. During sputter etching, both the BeO chip and the copper support plate are acted on with material removed from both of them. As a result, some of the removed copper from the plate contaminates the BeO substrate.

The overall phenomenon occurring at the ceramic surface in terms of surface chemistry is not understood and the ion microprobe results are not definitive. Sodium concentrations are particularly curious since their bulk level is very low compared to other binder additives which appear in lower quantities at the surface. Improper handling prior to analysis could have introduced salts which would appear at the surface. A more detailed review of cleaning treatments shall be conducted as a part of the next phase of this study.

3.4 Surface Roughness of the BeO Substrate with Various Preparation Treatments

The effects of pre-sputtering treatments upon the beryllia substrates surface roughness were studied with the aid of a scanning electron microscope (SEM). Surface topology for each of the following sample preparations was determined: as received, sputter etched, and 500°C and 1,000°C air firing. Figure 12 depicts the SEM photos for the studied treatments at 240X. For this analysis, one coupon was quartered (Q512) and each quarter used for only one of the above tests. The surface roughness of the coupon as a whole initially was 6 to 8 microinches rms, as measured using a profilometer.

SEM photographs reveal that the as-received, 500°C and 1,000°C air-fired portions of the coupon appear identical. This means that air firing removes only moisture and volatile lapping residuals without altering the surface finish of the substrates. Sputter etching, however, improves the surface

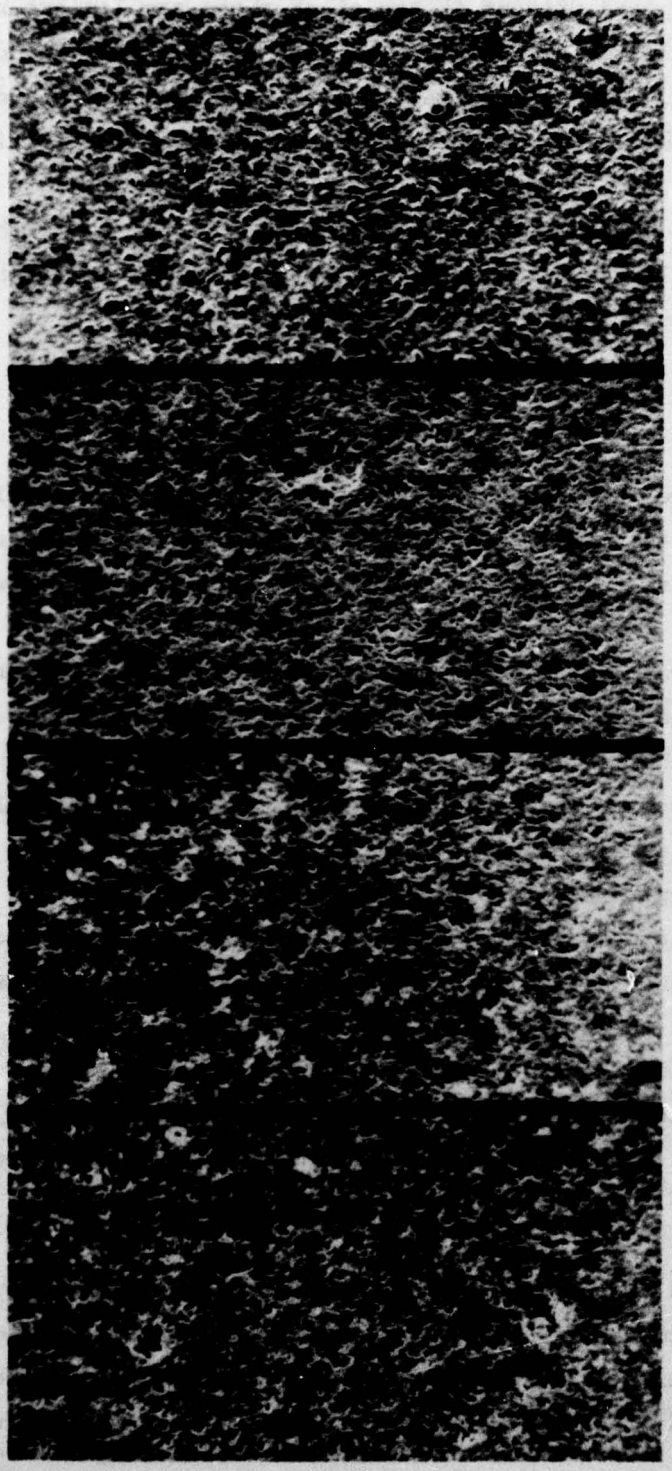

A. AS RECEIVED

B. SPUTTER ETCHED

C. 500 °C AIR FIRED

D. 1000 °C AIR FIRED

156-021302

Figure 12. SEM Photographs of BeO Substrate With Different Surface Preparation Treatments.

finish slightly. The high peaks present in the other three samples are reduced in the case of sputter etching. Figure 13 shows surface profile scans using a Dateck profilometer. The as-received chip (figure 13A) has a greater variation in surface roughness as compared to the sputter etched chip (figure 13B), where the total variation is markedly lower.

It can be concluded from the above that air firing does not alter the surface finish of the beryllia substrate and that sputter etching could be employed to reduce surface roughness of the beryllia substrate.

4. SPUTTERING PROCESS

4.1 Background

The relatively low power handling capability and high transmission losses associated with moly-manganese metallizing in the cfa led to a Warnecke-sponsored investigation for a new process with low thermal barrier resistance and low rf losses, eg,

A. an interface between ceramic and metal line as smooth as possible

B. a diffusion brazed copper interface that would avoid eutectic alloys which have high thermal resistivity

If thin films are necessary for the bond, the thickness must be small compared to the skin depth of the material.

In the first test, copper was evaporated in wet hydrogen, forming a copper oxide compound to a thickness of 25 μm. The oxide compounds were reduced to copper at the surface and a diffusion braze was tried. Copper diffused along the outer surface and through the BeO, resulting in higher rf loss and a degradation of the overall dielectric characteristics of the ceramic. In the next step, to prevent the diffusion of copper into the ceramic, a film of molybdenum, on the order of 5,000 Å, and a film of 50,000 Å of copper were evaporated on the substrate. The 5,000 Å molybdenum film was thinner than the skin depth at 3 GHz.

Between molybdenum and copper, negligible diffusion occurs, so that the copper will not diffuse into the BeO substrate. However, when a diffusion braze between the copper surface and copper was made, no adherence between molybdenum and BeO occurred; the evaporated films easily lifted off the underlying ceramic.

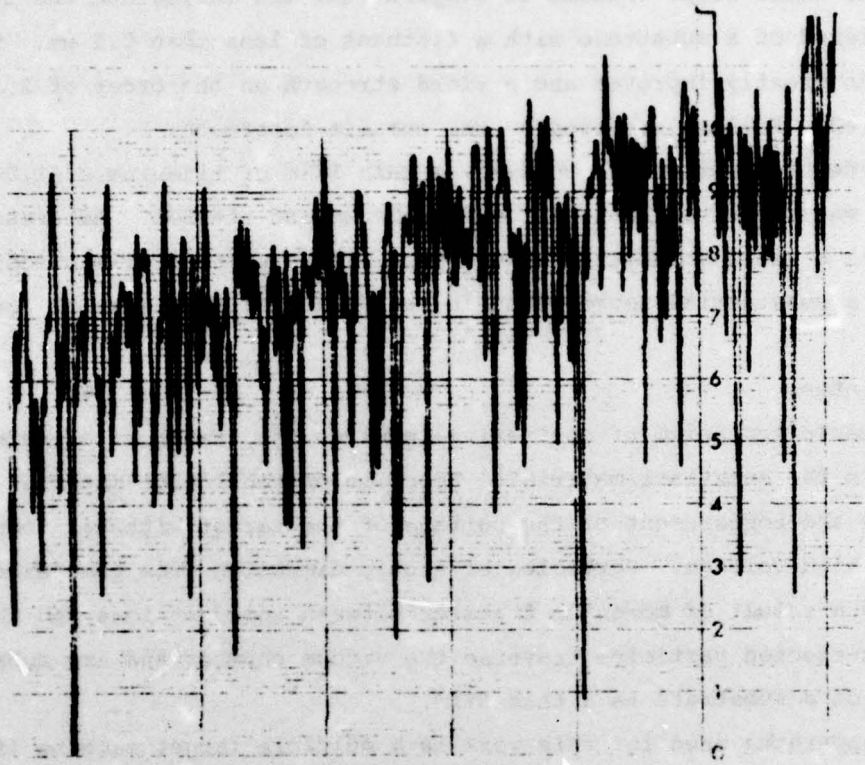

A. AS RECEIVED - 10 MICROINCHES RMS

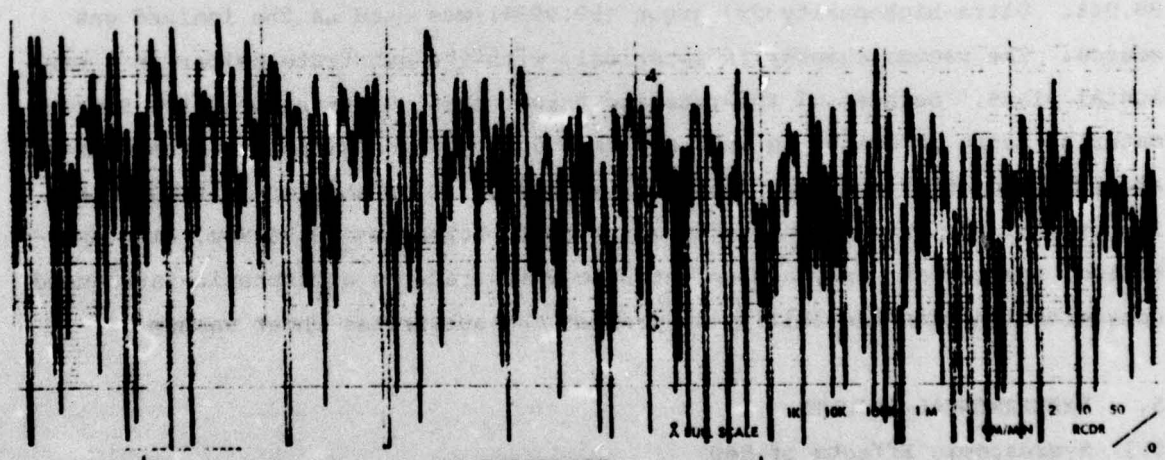

1 mm SUBSTRATE

B. SPUTTER ETCHED - 8.5 MICROINCHES RMS

RECORDER SPEED: 10 cm/min VERTICAL SCALE: 1000 Å/cm = 4 μin/cm

156-021303

Figure 13. Surface Profile of Beryllia Chip (Q512).

In the third step, instead of evaporation, the molybdenum and the copper were sputtered on a substrate with a flatness of less than 0.1 μm. The adherence was greatly improved and a yield strength on the order of 2,500 psi was measured. Failure occurred at the ceramic interface.

In order to improve the bonding, a thin film of titanium of 1,000 Å thickness was deposited between the molybdenum and the BeO. Adherence was improved with a yield strength of 4,000 psi. The sputtered film process did result in a substantial improvement in heat transfer and lower rf losses.

4.2 Apparatus

The basic mechanism of sputtering involves the transport of material from a target to the substrate material. Ejection of the source material is accomplished by the bombardment of the surface of the target with gas ions accelerated by high voltage. Particles of atomic dimension from the target are ejected as a result of momentum transfer between incident ions and the target. The target-ejected particles traverse the vacuum chamber and are subsequently deposited on a substrate as a thin film.

The apparatus used for this work is a multiple target machine (figure 14), with the 8-inch targets rotating on the face of a cube. The three targets and their purity used were: copper - 99.998%, molybdenum - 99.95%, and titanium - 99.94%. Ultra-high-purity dry argon (99.999%) was used as the ionized gas source. The vacuum chamber is spherical, with the substrate holder in a horizontal plane. Because of the rotating target configuration, only the source material being deposited is in the plasma during deposition; the other targets are shielded, thus reducing cross contamination to an absolute minimum. Key features of the unit are: rf sputtering up to 1.2 kV at 13.56 MHz, bias sputtering, sputter etching, and an intervac which reduces atmospheric-introduced contamination with the ability to preheat the substrates under vacuum.

5. EXPERIMENTAL RESULTS

5.1 Hygroscopic Effects of BeO

It is reasoned that the presence of moisture on the BeO surface will inhibit film formation by its vaporization when the first sputtered atoms reach the substrate. A series of BeO coupons were air fired at 1,000°C and sputtered after various delays at ambient conditions. The series consisted of 0-,

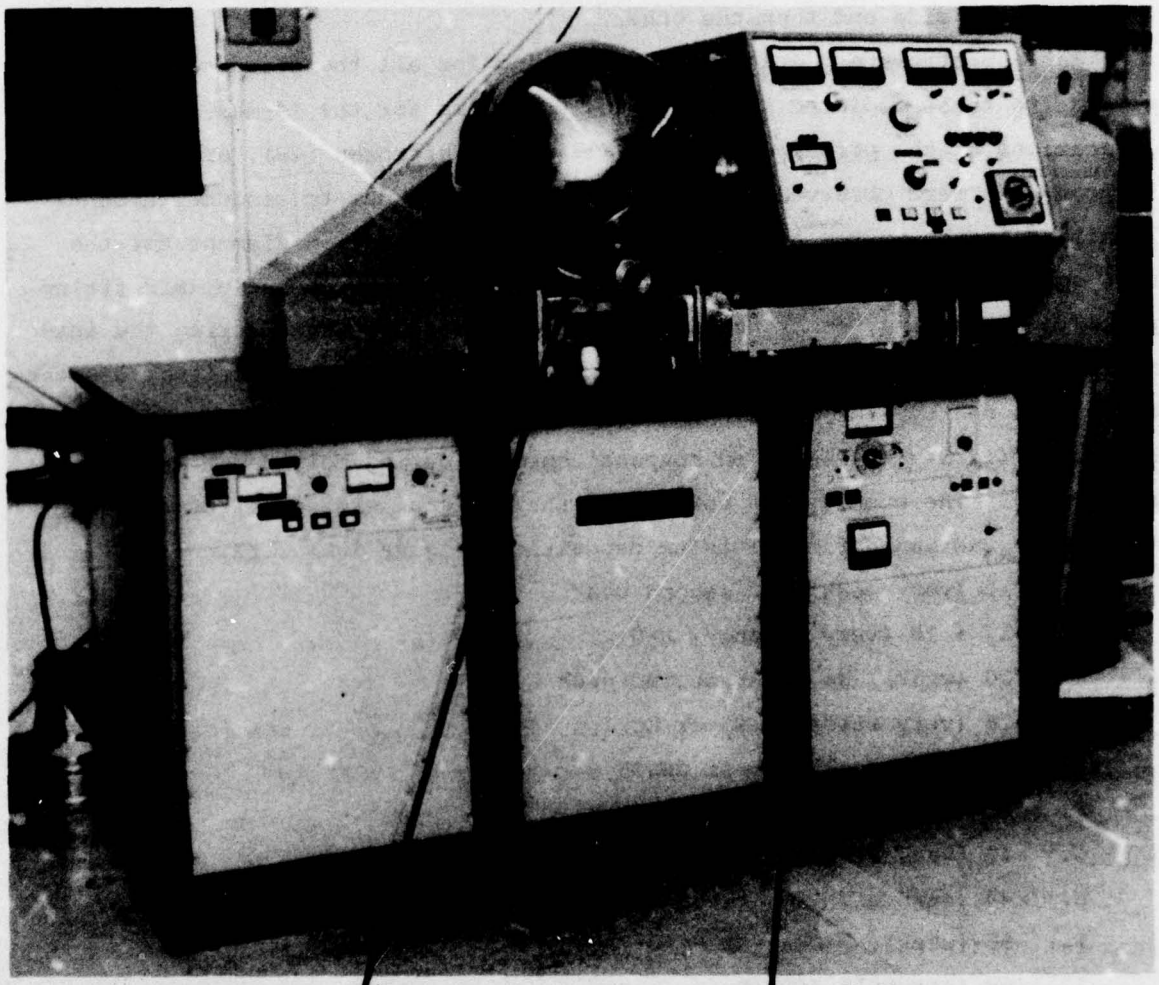

Figure 14. RF Sputtering Apparatus (MRC Sputtersphere, Model 822).

1-, 3-, 7- and 14-day delays before sputtering. All coupons were sputtered in the same fixture location. In addition to the air-fired delayed series, one coupon was sputtered without any air firing. The sputtering sequence consisted of laying down 1,500 Å of Ti, 5,000 Å of Mo, and 7 μm of Cu respectively on one side and then the other.

Mass spectrometer data during sputtering for all the fired coupons are similar to those depicted in figure 15, which are for the 14-day delay (Q516). Indications of the presence of water (17 & 18), nitrogen (28), argon (40) and krypton (84) were observed. The krypton is present due to residual amounts remaining in the system after it was used as a calibration element for the mass spectrometer. In the case of the coupon (Q519) which had no air firing prior to sputtering, numerous additional peaks were observed during the initial titanium sputtering (figure 16); after this stage, no additional elements other than the typical water, nitrogen and argon were observed, as indicated by the similarity to the fired coupons' spectra during molybdenum and copper sputtering. The atomic mass units (and their signal strengths) of the contaminants observed during titanium deposition (figure 16A) were:

A. 12 (very weak): CO second peak
B. 17 + 18 (very strong): H_2O
C. 20 (weak): Ne or Ar second peak
D. 28 (very strong): N_2 or CO
E. 32 (very weak): O_2 or CH_3OH
F. 36 (very weak): Ar third peak
G. 40 (very strong): Ar
H. 44 (strong): CO_2
I. 56 (weak): $(CH_3)_3CH$
J. 68 (strong): $(CH)_3O$
K. 84 (very weak): Kr
L. 87 (weak): ?

With no air firing prior to sputtering, surface contaminants consist mainly of organic compounds which are most probably imparted to the substrate during lapping and are embedded to a degree that simple ultrasonic solvent cleaning does not completely remove them. The contaminants appear instantaneously as the titanium is deposited and disappear quickly as the titanium

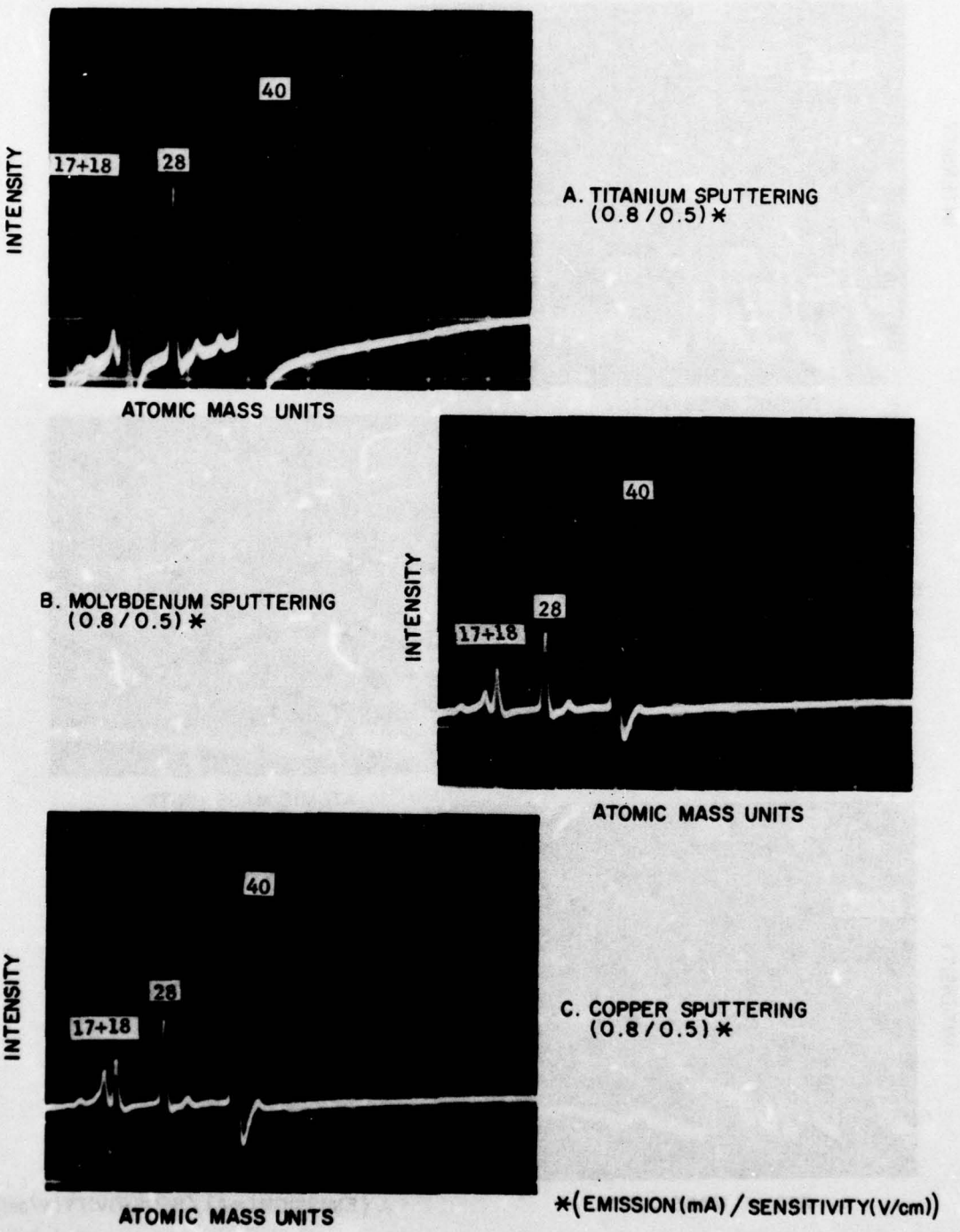

Figure 15. Mass Spectrometer Data During the Sputtering of Q516 (14-Day Delay After Air Firing).

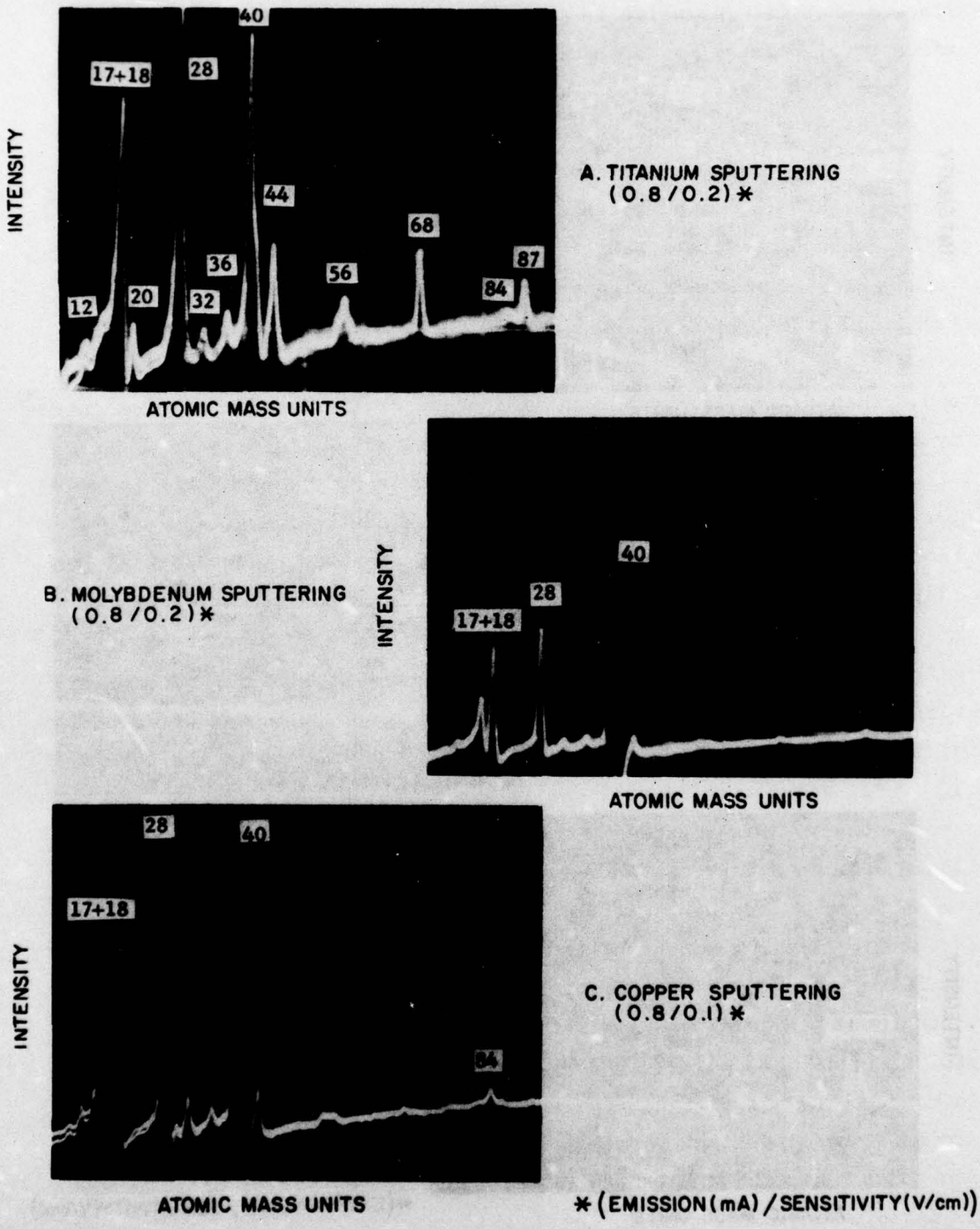

Figure 16. Mass Spectrometer Data During the Sputtering of Q519 (No Air Firing).

layer is built up. It is not certain whether the contaminants are sputtered off or whether they react with the titanium and are permanently trapped at the BeO surface. What is conclusive is that air firing at 1,000°C does deplete the surface of all contaminants that can be vaporized during sputter metallizing.

The effect of moisture on the bonding of sputtered films on BeO was tested. The average tensile stress results of these tests along with the standard deviation are shown in table 2 for different delays. Figure 17 is a plot of the average failure stress versus time delay; a trend exists that with longer delay time between air firing and sputtering, the tensile strength of the metallized ceramic bond is lower. An exception to the general trend is that with a 3-day delay, the tensile strength is markedly lower than the overall trend. This is an anomaly and an indication of the broad variation introduced by delaying sputtering after air firing and allowing moisture to reestablish on the hygroscopic substrate. Also noteworthy is that the standard deviation as a percentage of the average yield stress increases markedly with delay time. Not only does moisture reduce the bond strength attainable, but the variance in bond strength increases with moisture pickup.

The effect of the moisture on film morphology is also pronounced. Figure 18 shows the individual sputtered layers for one side of Q509 (no delay after air firing), as revealed by the electron microprobe technique. The individual layers are continuous and discrete. Figure 19 depicts the layers for Q518 (3-day delay after air firing). The titanium layer next to the BeO is not continuous. This represents the general phenomenon that the presence of moisture does interfere with the deposition and nucleation of uniform titanium. Figure 20 depicts the film layers for Q519, which did not experience air firing at all. Again the titanium has an island morphology and is not continuous. The ramifications of titanium are that without this active metal, bond strength is always lower than with it. When it is not continuous, its effect is reduced.

In conclusion, air firing, with its removal of hygroscopic water, appears to be a very important variable, with delay in sputtering resulting in a poor bond between the metallic-ceramic junction by virtue of a noncontinuous titanium layer.

Table 2. Tensile Test Data for Coupons With Delay After Air Firing Prior to Sputtering.

Coupon	Delay (Days)	Tensile Failure (psi) Average of 3 Tests X	Standard Deviation σ	Percentage $\frac{\sigma}{X}$ X100
Q509	Zero	11,699	579	5
Q513	1	9,757	1,058	10
Q518	3	4,015	809	20
Q515	7	7,027	1,551	22
Q516	14	5,152	1,279	25
Q519	No Firing	6,705	2,078	31

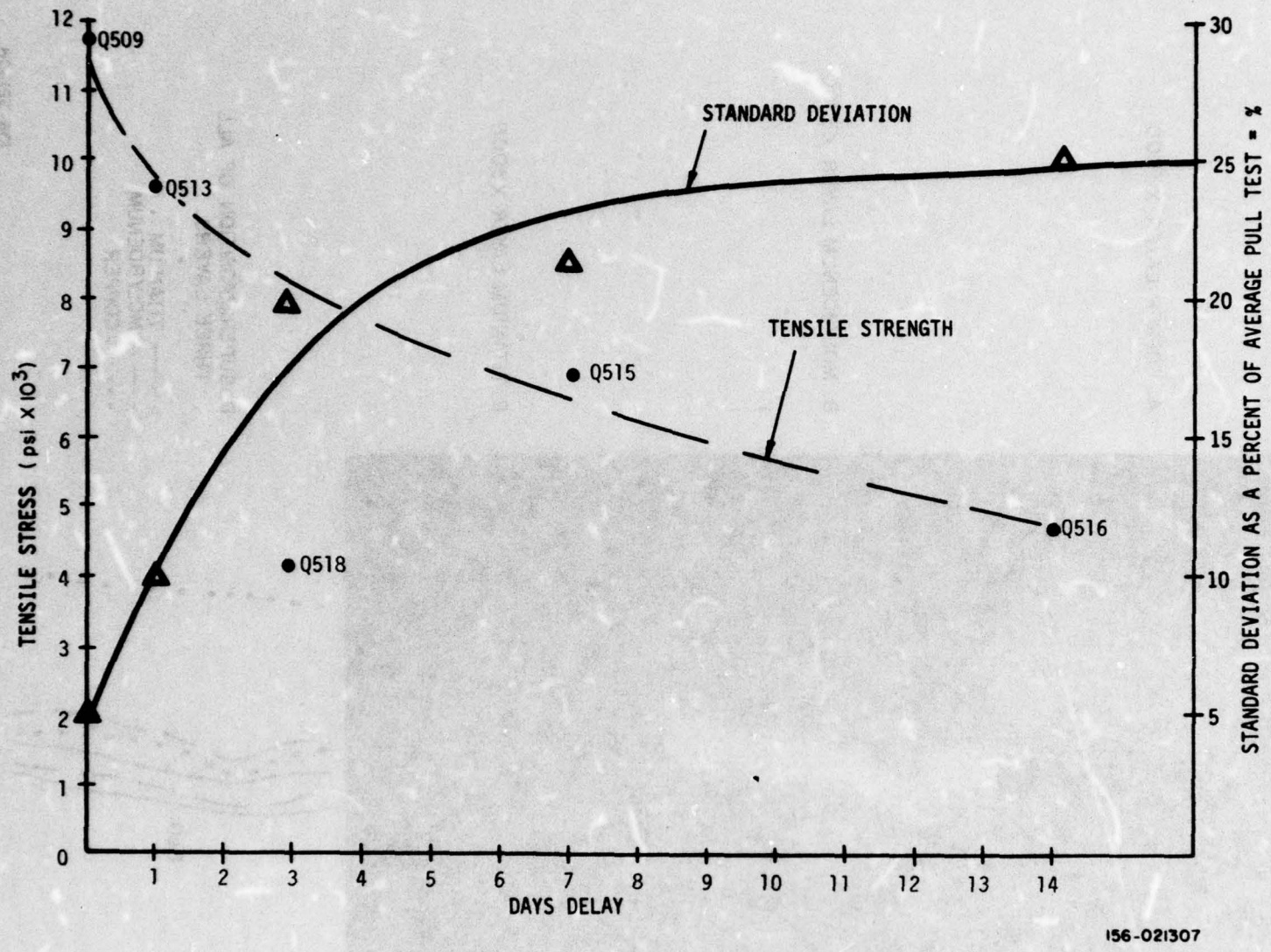

Figure 17. Failure Tensile Stress Versus Days Delay After Air Firing Prior to Sputtering.

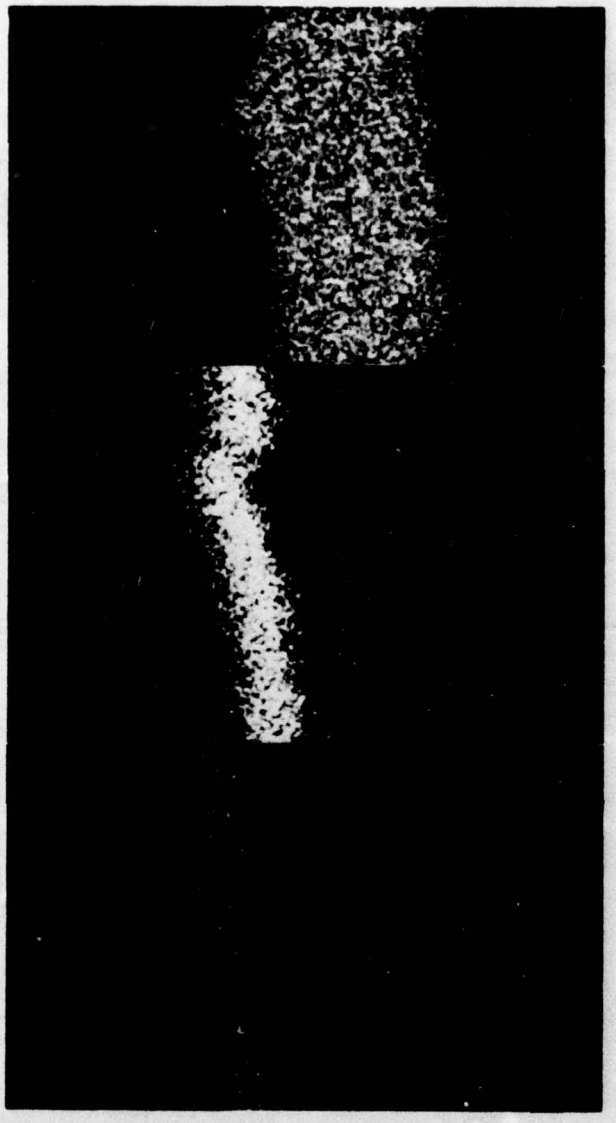

A. COPPER LAYER X3000

B. MOLYBDENUM LAYER X3000

C. TITANIUM LAYER X3000

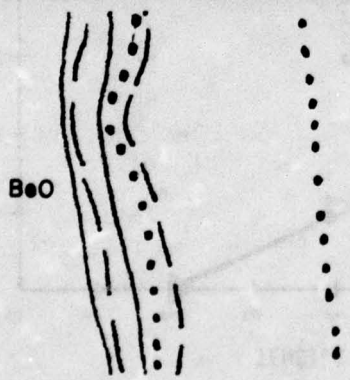

D. SUPERIMPOSITION OF ALL THREE LAYERS.

——— TITANIUM
– – – MOLYBDENUM
•••••• COPPER

156-021308

Figure 18. Film Morphology for Q509, Air Fired, No Delay, Side 1, As Sputtered.

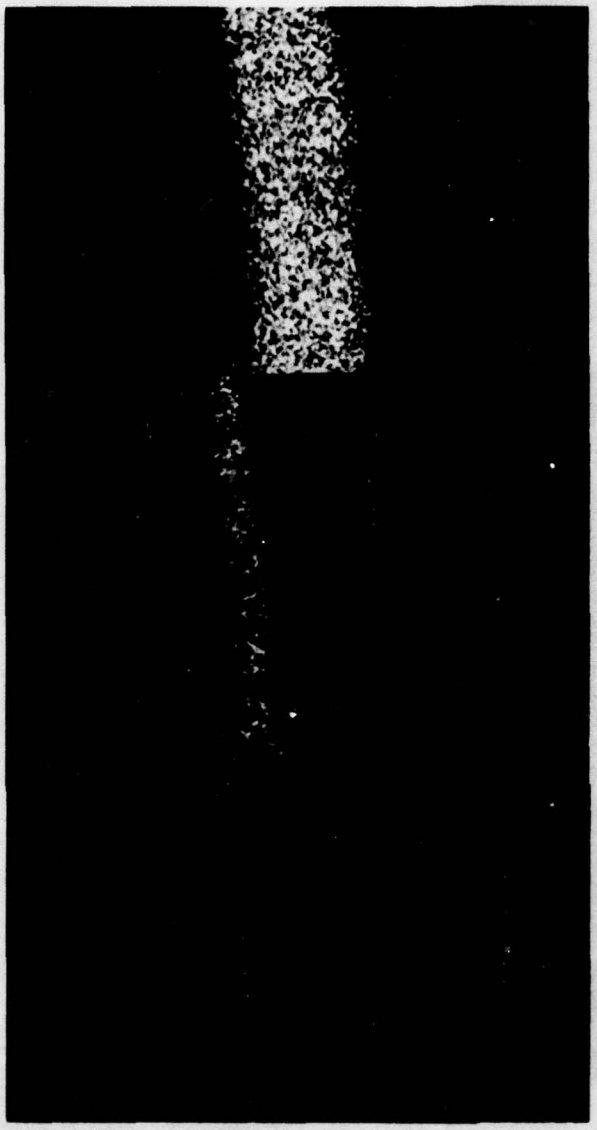

A. COPPER LAYER X3000

B. MOLYBDENUM LAYER X3000

C. TITANIUM LAYER X3000

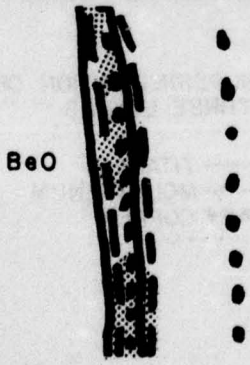

D. SUPERIMPOSITION OF ALL THREE LAYERS

——— TITANIUM
– — – MOLYBDENUM
• • • • • COPPER

156-021309

Figure 19. Film Morphology for Q518, Air Fired, 14-Day Delay, Side 1, As Sputtered.

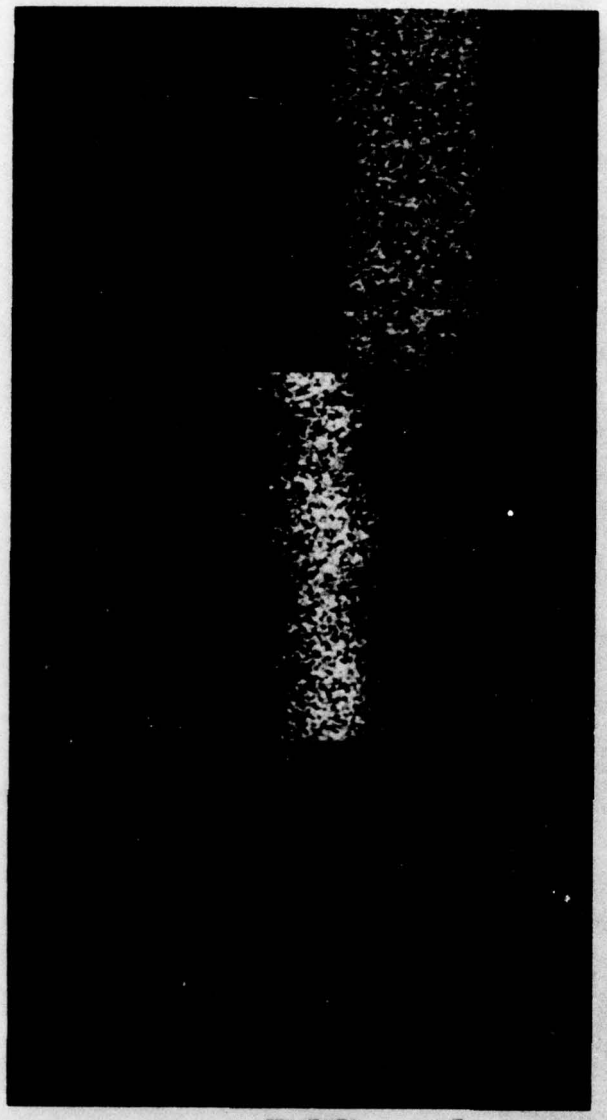

A. COPPER LAYER X3000

B. MOLYBDENUM LAYER X3000

C. TITANIUM LAYER X3000

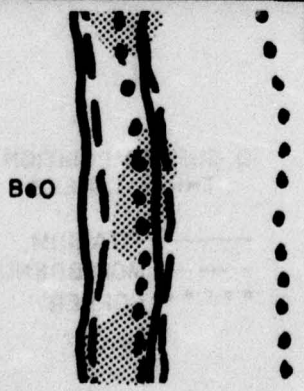

D. SUPERIMPOSITION OF ALL THREE LAYERS

——— TITANIUM
— — — MOLYBDENUM
●●●●● COPPER

156-021310

Figure 20. Film Morphology for Q519, Not Air Fired, Side 1, As Sputtered.

5.2 Copper Sputtered on Beryllia

Previously, copper had been evaporated in wet hydrogen, forming a copper oxide that was subsequently reduced in dry hydrogen. After brazing to copper rods it was observed that the copper had diffused into the BeO and along the outer surfaces, thus degrading the dielectric properties. In an attempt to duplicate these findings using sputtering, a coupon was air fired and placed in the sputtering chamber with no delay. Each side of the coupon was sputtered with 9 μm of copper. Next, three ¼-inch-square pieces were brazed and pull tested. The strength of the copper-to-BeO bond was only 1,360 psi. Failure occurred at the BeO surface. Penetration of the copper into the BeO was negligible. The sputtered copper film could be peeled from the ceramic only in the area of the knife contact (C rating).

The results of sputter deposition were not the same as for copper oxide reduction in terms of copper penetration into the BeO. Reduction of CuO/Cu_2O on BeO would not necessarily result in oxygen-free copper; what may result is eutectic formation of Cu_2O and melting at 1,065°C. This phenomenon is the same mechanism used by General Electric's[8] proprietary process of bonding copper directly to ceramic. By sputtering oxygen-free copper onto BeO and brazing in hydrogen, no eutectic can be formed at the BeO surface below the exposed copper. The ramification is that sputtered oxygen-free copper does not readily penetrate BeO at high temperatures, nor is there any bonding enhancement in addition to the sputtering momentum of individual atoms. Pure copper alone cannot be sufficiently bonded by sputtering and brazing to BeO to be employed at this time in high power microwave tubes.

5.3 Molybdenum Plus Copper Sputtered on BeO

5.3.1 Metallic Layer Thickness Resolution. The solubility of copper in molybdenum is virtually nil, even above the melting point of copper (1,083°C). For this reason, molybdenum was selected as a diffusion barrier. The optimum molybdenum thickness is a tradeoff between that necessary to prevent any copper migration and as little as possible to reduce the attenuation effects of molybdenum on rf microwaves due to the skin effect.

[8] Burgess, J.F., and Neugebauer, C.A., "Hybrid Packages by the Direct Bonded Copper Process," Solid State Technology, May 1975, p 42-44.

Three samples were sputtered with varying molybdenum thickness to be compared to the calculated optimum of 5,000 Å. The samples had: no molybdenum, one-half the thickness (2,500 Å), and twice the thickness (10,000 Å). Electron microprobe analysis was used to ascertain copper penetration through the molybdenum layer. The samples were examined in the as-sputtered state and also after a 1,000°C soak for 24 hours. The sample with no molybdenum (Q530) had some copper penetration into the BeO after the elevated temperature soak (figure 21). With only 2,500 Å of molybdenum, the amount of copper penetration into the BeO was reduced, but it did move through the molybdenum layer in appreciable amounts (figure 22). With 5,000 Å of molybdenum, no detectable penetration of copper was observed. The same held for 10,000 Å of molybdenum.

The high temperature excursion of 1,000°C is required to produce a copper-copper diffusion braze in reasonable times for fabrication of microwave tubes. A layer thickness of 5,000 Å of molybdenum is necessary and sufficient to inhibit copper diffusion at this required temperature. Using an increased amount of molybdenum should be avoided, since it will also increase the attenuation experienced during microwave propagation.

5.3.2 Sputtered Bond Failure Characteristics. Deposition of 5,000 Å of molybdenum and 7 μm of copper (Q520) produced a bond strength of only 2,000 psi. Failure occurred at the ceramic-metallic interface, with no evidence of ceramic fracture. Bond strength degradation with thermal cycling was catastrophic. Table 3 is a summary of the tensile strengths for Q520 with thermal cycling at 500°C after diffusion brazing of copper rods. Figure 23 depicts the overall tendency for bond deterioration with cycling. The mode of failure remains constant - ceramic-metallic interface separation.

The tendency for weakening bond adhesion with thermal cycling can be attributed to the thermally induced stresses of the expansion and contraction of the metals relative to the BeO. Bonding between the metallic layers remains intact, but the tendency for complete separation after only 25 cycles prevents the use of this process for microwave tube utilization. Given the mode of failure, the metallic layers will become free along with any structure brazed to them. Heat transfer will become very poor as the conductive path is interrupted. The end result will be a lifting of the delay line itself into the electron beam, with ultimate melting and a catastrophic tube failure.

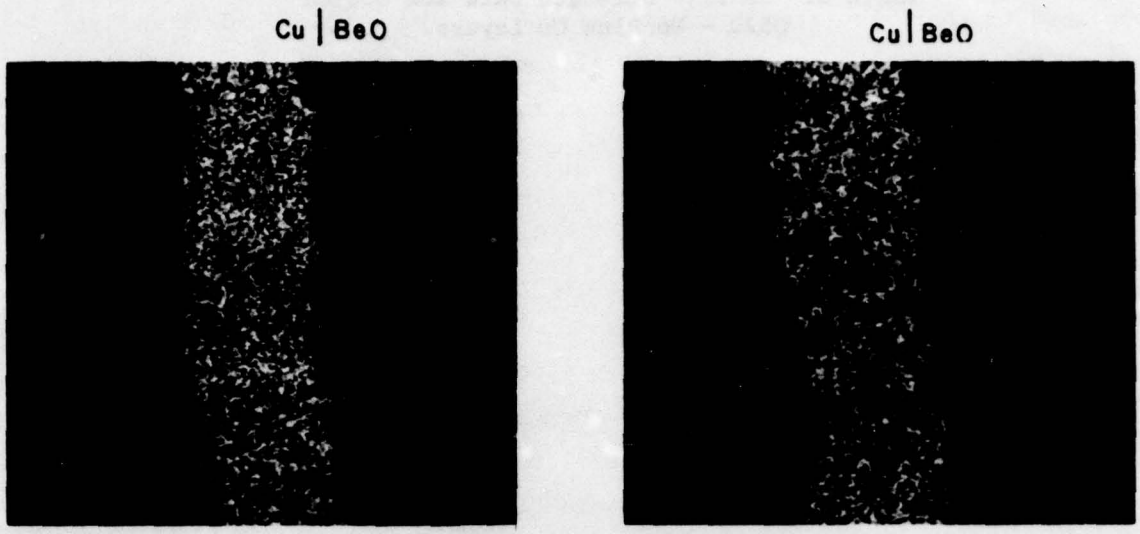

A. AS SPUTTERED

B. 1000°C FOR 24 HOURS

156-021311

Figure 21. Copper Distribution for Q530, No Molybdenum (X3000).

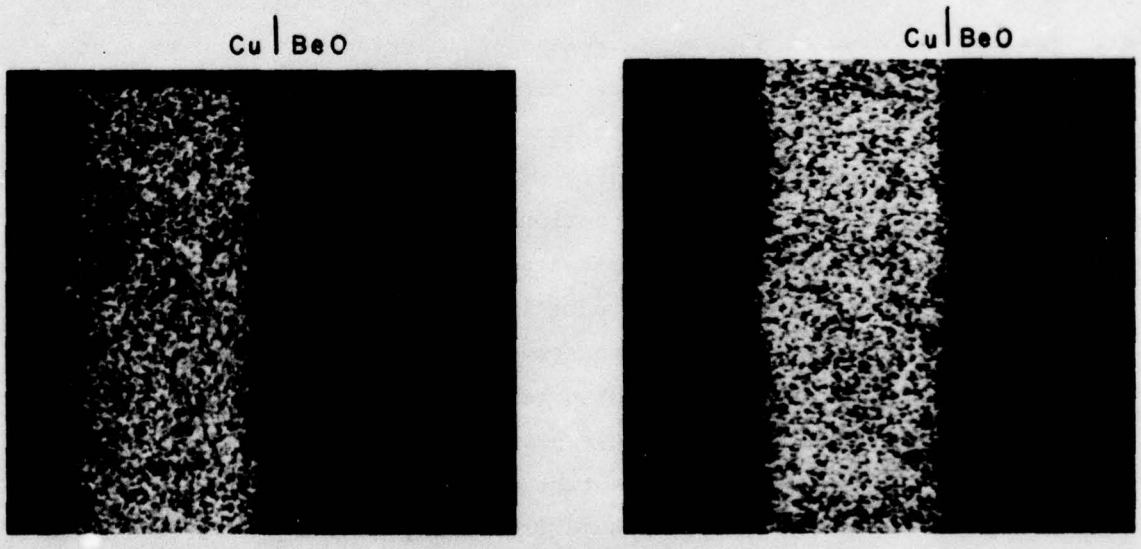

A. AS SPUTTERED

B. 1000 °C FOR 24 HOURS

156-021312

Figure 22. Copper Distribution for Q527, 2500 Å of Molybdenum Between Cu and BeO (X3000).

Table 3. Tensile Strength Data for Coupon Q520 - Mo Plus Cu Layers.

Cycles at 500°C	Average Tensile Strength (psi)	Standard Deviation (psi)	Peel Test Results Side 1/Side 2
0	1987	473	A/A
5	1934	1677	A/A
15	471	683	A/A
25	0	0	A/A

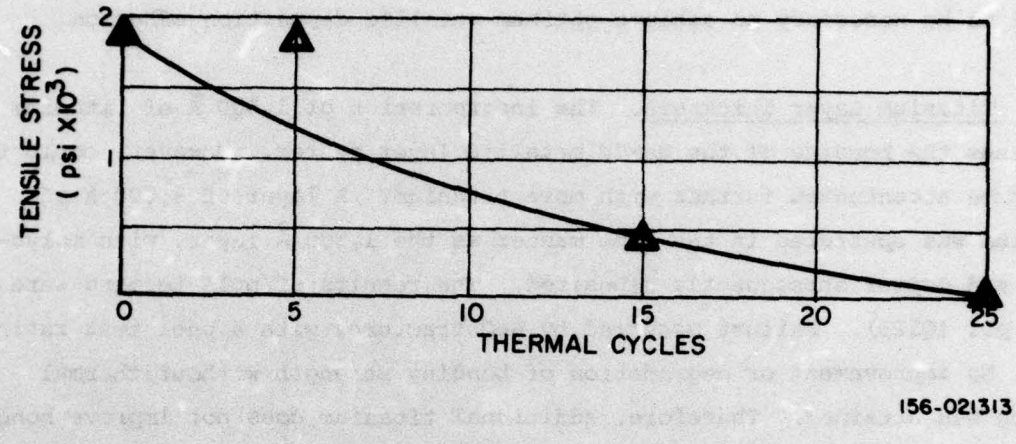

Figure 23. Tensile Failure Stress Versus Thermal Cycles for Coupon Q520 with Molybdenum and Copper Only.

5.4 Titanium-Molybdenum-Copper Sputtered on BeO

5.4.1 Introduction of an Active Metal Layer. The introduction of an active metal such as titanium is intended to enhance metallization by providing an interfacial zone which forms a continuous layer that nucleates and forms in such a manner that the oxygen supplied by the oxide ceramic is chemically reactive with the active metal[9]. In essence, the phenomenon is one where the active metal shares the oxygen of the ceramic and penetrates to a depth below the surface governed by atomic radii. The result is a gradual transition from active metal oxide to pure metal which provides a favorable surface for subsequent metallic layer bonding.

A sample (Q546) of BeO was sputtered with 1,500 Å of titanium, 5,000 Å of molybdenum, and 7 μm of copper on both sides. Tensile strength of the bond witout cycling was 9,420 psi. The mode of failure was ceramic fracture in the area of contact below the copper rod. This is an indication of excellent

[9] Mattox, D.M., "Thin Film Metallization of Oxides in Microelectronics," Thin Solid Films, 18 (1973) p 173-186.

bonding where the tensile strength of the BeO is the limiting factor in pull test stress measured. Peel strength testing revealed a very tenacious bond (A rating both sides).

Given the remarkable improvement in bonding of the sputtered layers with the addition of a very thin coating of titanium, an active metal layer is judged to be necessary to achieve optimum metallic deposition adhesion.

5.4.2 Titanium Layer Thickness. The incorporation of 1,500 Å of titanium increases the bonding of the Mo-Cu metallic layer system. However, could this effect be accentuated further with more titanium? A layer of 3,000 Å of titanium was sputtered in the same manner as the 1,500 Å layer, with molybdenum and copper subsequently deposited. The results of pull testing were 8,580 psi (Q525). Failure occurred by BeO fracture, with a peel test rating of A. No improvement or degradation of bonding strength without thermal cycling was attained. Therefore, additional titanium does not improve bonding beyond the role it plays in forming an oxide-to-metallic transition region for subsequent layer deposition.

5.4.3 Effects of Poor Initial Vacuum. During sputtering, argon is introduced into the chamber through a controlled leak. The nominal pressure during sputtering is 5×10^{-3} torr to 10×10^{-3} torr. Prior to the introduction of argon, the vacuum in the chamber should be as good as possible. The rationale is that the better the vacuum, the lower the concentration of possible contaminants which may react during sputtering by virtue of the heat generated and be introduced into the films during deposition. The concentration of contaminants is also a function of time at lower than ambient pressure; hence, the use of an intervac for sample insertion reduces the overall contamination level because the chamber is always under high vacuum.

To ascertain the effect of ultimate vacuum on sputtered film bonding in the Ti-Mo-Cu system, a sample (Q523) was sputtered with a less than maximum ultimate vacuum by introducing argon during pump down. The ultimate vacuum was 5×10^{-4} torr compared with conventional vacuums of less than 5×10^{-6} torr. Resultant pull-test strengths were only 4,830 psi, or roughly half that of those obtained when the ultimate vacuum exceeded 10^{-5} torr. The result is double that experienced without titanium but it does highlight the importance of condensible contaminants and their sinister influence on film adhesion.

5.4.4 Residual Stresses. Theoretically, the metallic layers are applied hot by sputtering, and upon cooling to room temperature a tensile stress can result in the metallic layers because of the differing thermal expansion coefficients of the metals relative to the BeO ceramic substrate. That is, the ceramic acts as rigid constraint on the contraction of the metals upon cooling. The higher the temperature experienced during sputter deposition, the greater the contraction, if the metal is free to do so. When the metal is constrained at one side, a residual compressive stress will be imparted to the substrate. The camber or amount of bending of the overall structure is a direct indication of the elastic deformation which results from the residual stress acting on the composite, assuming that the metal film is uniform over the whole coupon.

Experimentation to review the amount of thermal residual stresses imposed on a coupon during sputtering consisted of sputtering only one side of a coupon and measuring the camber. Coupons Q514, Q517, and Q524 were selected because of their insignificant initial camber, which was less than 0.0001 inch overall prior to sputtering. All samples were air fired at 1,000°C for 30 minutes. Sample Q514 was measured after the air firing and showed no net change in flatness, signifying that uniform air firing does not alter coupon flatness and that no residual stresses exist in the coupons prior to sputtering. Coupon Q517 was sputtered with no water cooling in the anode plate below the coupon, while water cooling to the target was maintained. Maximum temperature of the cooling platform was 75°C during the copper deposition. Coupon Q524 was sputtered in the same manner as Q517, except the additional water flow through the substrate holder kept the temperature below 24°C during the whole sputtering sequence. Table 4 summarizes the results of the camber measurements. The change in flatness is a result of tensile stress in the metallic films, causing them to rise (convex when viewed from the metal surface). Coupon Q517, which was sputtered hotter, does display a greater camber as evidence of a higher residual stress compared to Q524.

In an attempt to relieve the residual stresses, the coupons were fired at 500°C in wet hydrogen and after one-half hour showed no significant change. After an additional 24 hours no additional change was observed. The significance of this result is that 500°C is insufficient to relieve thermally induced residual stress even after 24 hours. Next the samples were fired at

Table 4. Camber Measurements of Coupons Sputtered on Only One Side.

	CAMBER OVER ENTIRE COUPON (INCHES)*		
	Q514	Q517 (No Water Cooling)	Q524 (Water Cooling)
Before Air Firing	0.0001	0.0001	0.0001
After Air Firing @ 1000°C/30 Min	0.0001	------	------
After Sputtering	------	0.00045	0.00020
After 500°C Firing 0.5 Hour in H_2 Wet	------	0.0005	0.0002
After 500°C Firing 24 Hours in H_2 Wet	------	0.0005	0.0002
After 1000°C Firing 24 Hours in H_2 Wet	------	0.0003	0.0003

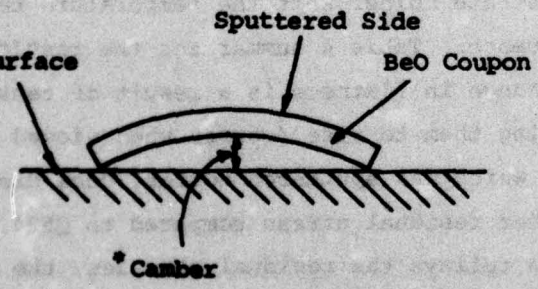

1,000°C, the diffusion braze temperature, for 24 hours to see if any changes occurred. Some degree of relaxation did occur but the samples did not return to their original flatness. The conclusion is that the degree of camber introduced which cannot be relieved at 1,000°C is permanent.

At present, the conclusion is that the degree of residual stress is a function of the temperature of metallic film deposition. Low residual stresses are desirable because of the internal strain experienced within the layers at ambient conditions and because upon heating, these stresses are additive to thermally induced stresses. The metallic layers are in tension by virtue of the residual stress. The ceramic substrate is in compression. Upon heating, the stress in the films increases relative to the ceramic and could result in separation. These effects are believed to prevent maximum bond strength formation and tend to exhibit themselves in reduced resistance to thermal fatigue.

5.4.5 Sputter Etching of BeO Substrate. Sputter etching of the BeO substrate was shown to reduce surface roughness to some degree. Therefore, it appears that this technique could be beneficial in terms of rf losses. The cleaning action of sputter etching may also be a means of improving sputtered film bonding. A coupon was processed in the same fashion as Q546, in the standard sequence, with sputter etching performed prior to the deposition of titanium. The pull-test results for this effort (Q534) were 8,700 psi. Film morphology is similar to coupons without sputter etching - each layer is discrete and continuous. No real improvement in bond strength was realized. Perhaps the initial roughness provides some degree of mechanical locking mechanism. Perhaps air firing removes all contaminants that impair film bonding and sputter etch does nothing additional. In any case sputter etching did not offer any bond strength improvements.

5.4.6 Bias Sputtering of Titanium. Bias sputtering has been used in the semiconductor industry as a means of depositing a denser film, often with preferential crystal orientation[10]. The technique consists of placing a small

[10] Maissel, L.F. and Glang, R., Handbook of Thin Film Technology, McGraw-Hill, 1970, p 4-22.

negative potential on the substrates, causing some degree of back sputtering during deposition. It generally affects the composition and structure of deposited coatings. Through the back-sputtering mechanism, undesirable gas entrapment tends to be reduced.

Realization of a continuous titanium coating is a known objective for achieving tenacious bonds to BeO. Bias sputtering with its inherent denser coating was though to be a plausible route to improving the bonding of the metallic system under study. A coupon (Q535) was sputtered using a 10% bias during the deposition of titanium only. Continuous film morphology was achieved. However, the tensile strength of the overall metallic composite was very poor. A pull-test average of three separate tests was 1,480 psi.

An explanation for the failure of bias sputtering to produce tenacious bonds lies in a momentum consideration of the atoms sputtered into the ceramic substrate. Given negative biasing as a retarding force, it reduces the impact velocity of atoms originating at the target directed at the substrate. The net effect is an overall reduction of the energy with which the sputtered atoms arrive at the ceramic surface. This reasoning is based on the premise that the higher the net velocity of atoms arriving at the ceramic surface, the deeper they are driven into the surface layer of the substrate. It is believed that this premise is valid because unwanted atoms present due to poor vacuum also interfere with the sputtered atoms, and as a result, less than optimum bonding occurs.

Gas entrapment in the sputtered films is not a problem, since the electron and ion microprobe analyses have shown that no detectable amounts of any gas contaminants are present within the films. Bias sputtering, however, cannot be totally dismissed; the only valid conclusion is that a 10% bias is excessive for the metallic-ceramic system under study.

5.4.7 <u>Diffusion of Titanium</u>. Previously, the degradation of the metallic bonds on sputtered BeO has been viewed as a fatigue phenomenon resulting from thermal stresses caused by the differences in thermal expansions between the layers. Evidence now points to the interaction of copper and titanium as the cause of bond deterioration. The purpose of molybdenum in the multilayered structure is to serve as a diffusion barrier for copper, and in principle, due to their essentially total insolubility, does achieve this function. But

molybdenum does not provide a sufficient diffusion barrier for titanium. Table 5 is a summary of volumetric diffusion data for the three principal metals used in the sputtered system. Whenever coefficients are given, they were used to calculate the volume diffusion coefficients as a function of temperature at 500°C and 1,000°C according to

$$D = D_o \exp \quad (-Q/RT)$$

where D and D_o are diffusion coefficient and frequency factor, respectively, usually given in cm^2/s; Q is the activation energy for diffusion, and R and T are the gas constant and absolute temperature in Kelvin respectively. Whenever coefficients D_o and Q are not given in the table, the value of D is taken directly from the literature.

Diffusion of titanium at 1,000°C through molybdenum is appreciable, and once through, the mobility in copper is very high even at 500°C. This diffusion of titanium through molybdenum and into the copper was confirmed using the ion microprobe technique on a pull-test assembly of sample Q513. The assembly experienced the copper diffusion brazing temperature of 1,015°C and 15 cycles between 25°C and 500°C. Failure occurred at 3,400 psi. This particular sample was selected because of the marked reduction in tensile strength from the samples which were not thermally cycled (average pull-test strength of 9,800 psi) and because visual examination revealed what appeared to be failure between the copper rods and the sputtered copper on most of the rectangular contact points. Figure 24 is a schematic representation of the separated pull-test assembly after tensile failure and designates the alphabetical coding used for each contact point.

Table 5. Diffusion Data for Selected Binary Systems.

System*	Diffusion Coefficient D_o (cm^2/s)	Activation Coefficient Q (kcal/g-atom)	Reported Temperature Range of Applicability (°C)	Volume Diffusion D (cm^2/s) at 500°C (773°K)	Volume Diffusion D (cm^2/s) at 1000°C (1273°K)	Ref
Cu : Ti	2.1×10^{-3}	29.2	Low Temp	1.08×10^{-11}	----------	11
	11.3	60.2	High Temp	----------	4.7×10^{-10}	11
Cu : Mo	----------	----	900	----------	9.3×10^{-11}**	12
Mo : Ti	2.5×10^{-2}	47.0	820-1600	1.13×10^{-15}	1.9×10^{-10}	13
	2.8×10^{-4}	33.2	900-1100	1.06×10^{-13}	5.3×10^{-10}	14
Ti : Mo	6.3×10^{-6}	50.5	820-1600	2.91×10^{-20}	1.24×10^{-14}	13

* X : Y, Host Species: Transformed Species; Read Y Into X

** Reported Value

[11] Caloni, O., and Strocchi, P.M., "Diffusion of Copper in Beta Titanium," Electrocim Metallorum, January 1969, 4, (1), p 45-48.

[12] Diffusion Data, Volume 2, Diffusion Information Center, 1968, p 121.

[13] Diffusion Data, Volume 4, Diffusion Information Center, 1970, p 318.

[14] Diffusion Data, Volume 1, Diffusion Information Center, 1967, p 39.

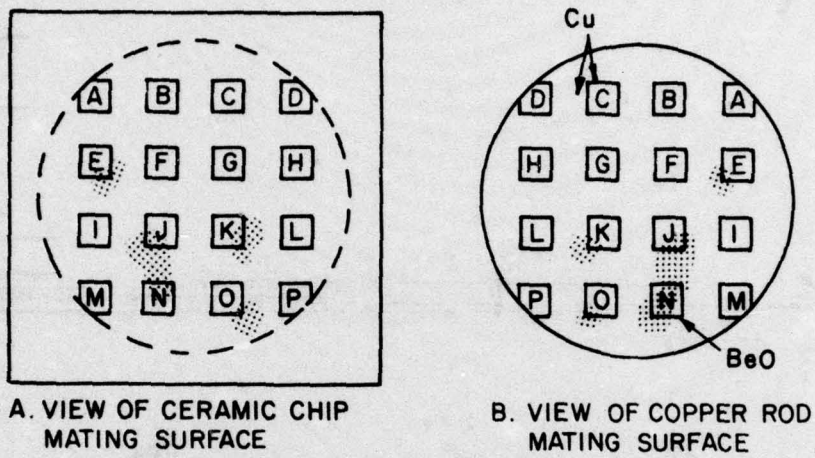

Figure 24. Schematic Representation of Pull Test Assembly After Separation.

Figures 25 and 26 are ion microprobe data for Q513 at position C both on the chip and the rod. On both the chip and the rod, titanium and copper are in evidence, but no molybdenum was detected. The presence of sodium, magnesium, and potassium is believed to result from salts through sample preparation and handling. In addition to the scan at position C, each rod location (except J, which was removed in order to perform the analysis) was focused onto, and constant time counts for titanium signals were taken. A summary in ranked order of the average of five separate counts at each position on the rod is presented in table 6. Large quantities of titanium were detected at each position, with no significant measures of molybdenum. This proves conclusively that titanium diffuses through the molybdenum layer and well into the copper sputtered layer. This also supports the fact that failure occurred within the copper and not at any boundary between the metallic layers.

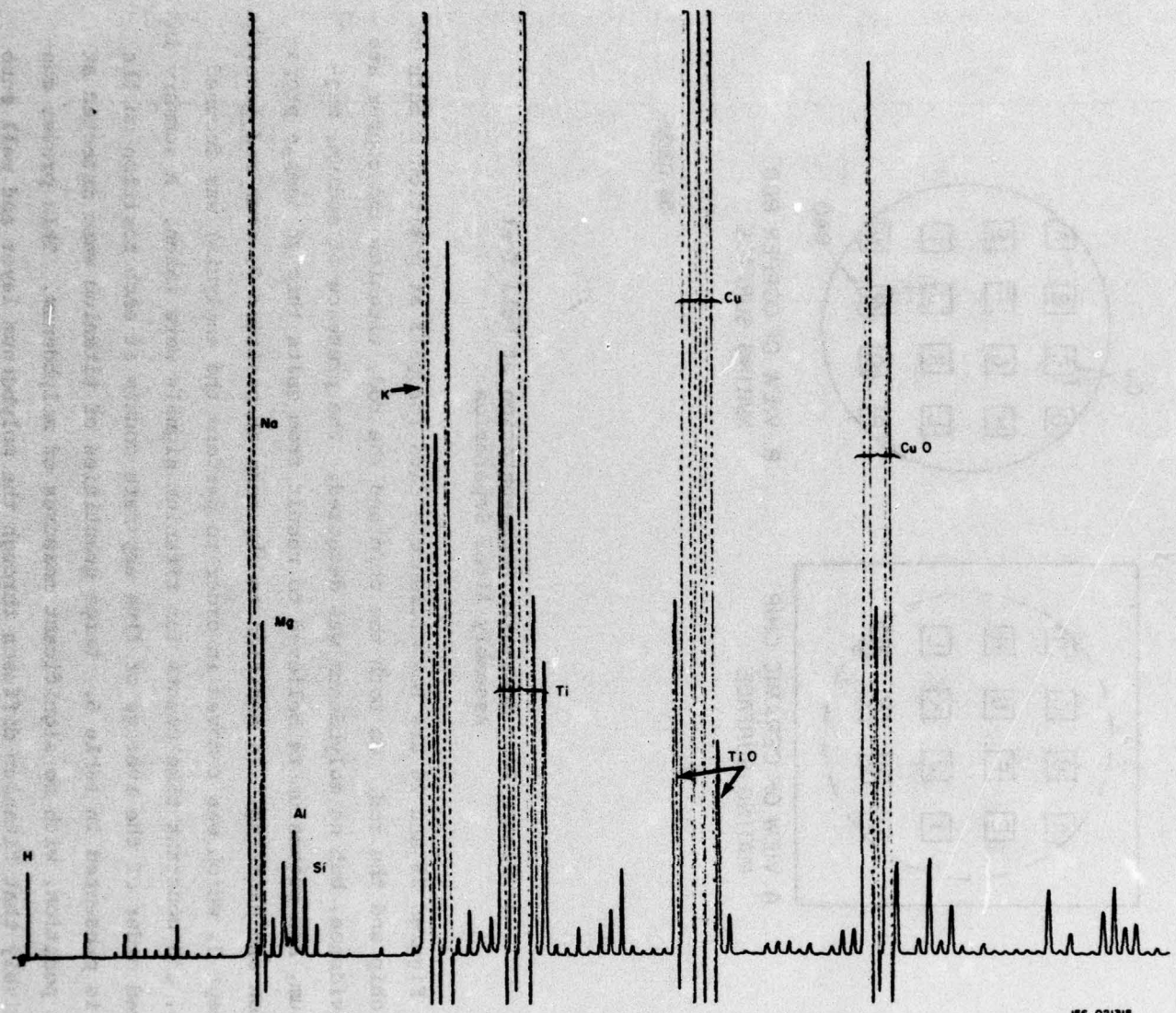

Figure 25. Ion Microprobe Data for Position C on Coupon Q513 (Chip).

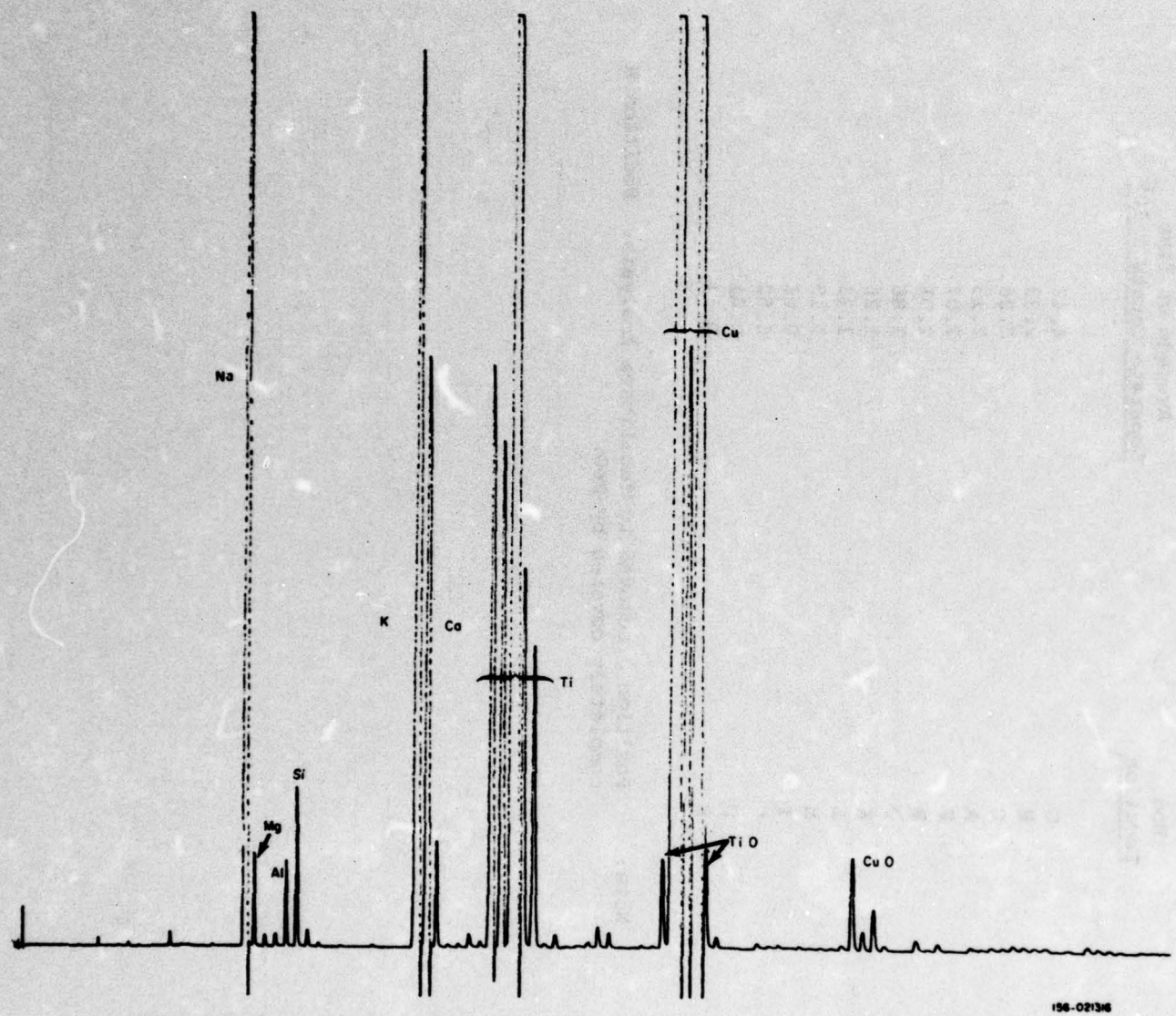

Figure 26. Ion Microprobe Data for Position C on Coupon Q513 (Rod).

Table 6. Average Counts Representing the Level of Detected Titanium at the Rod Locations for Q513 No. 10 (Ranked in Descending Order of Titanium Present).

Rod Location	Average of Five Separate Counts X 10^6
G	4.42
H	2.33
C	2.26
A	2.13
F	2.07
B	2.01
O	1.88
K	1.26
L	1.23
M	1.19
I	0.61
P	0.52
D	0.41
E	0.11

Note: Position J removed to facilitate analysis. Position N completely covered by BeO.

Titanium does diffuse through the molybdenum and into the copper (figure 27) and titanium and copper do form numerous intermetallic compounds. These intermetallics are brittle non-load-bearing constituents, which explains the deterioration in tensile strength of the bond and the change in failure mode with thermal excursions. Figure 28 shows the change in failure modes in tensile strain with thermal cycling. The failure mode without thermal cycles is one of rupture of the underlying ceramic. Tensile strengths are on the order of the tensile strength of the BeO, between 10,000 psi and 15,000 psi. After thermal cycling, the strength is reduced and the failure occurs as a result of breakdown of the copper-copper diffusion braze. Electron microprobe analysis (figure 27) shows the titanium which has diffused along the copper grain boundaries and colonized as intermetallic at the largest grain boundary - between the sputtered copper and the copper rods.

Further support to the deleterious effect of titanium migration is that when OFHC copper shims were used as substrates the following was observed: when a shim alone was brazed to pull-test rods, a bond formed which had a strength in excess of 20,000 psi, even after 25 thermal cycles. When copper was sputtered on the shims and then brazed, the same strength levels were seen. When the standard sputtered layers of titanium-molybdenum-copper were sputtered on a copper substrate, brazed, and pull tested, a tensile failure of about 8,500 psi was recorded. This is comparable to the results achieved with BeO, but well below that of copper alone. Finally, titanium alone was sputtered on one side of a copper substrate. Pull test results were on the order of 2,900 psi. This greatly reduced tensile strength is comparable to standard sputtered BeO after thermal cycling. The fact that titanium led to pull strengths of such a low value, coupled with the thermal cycling failure experienced with composite sputtered coupons, points to the critical effect of titanium interaction with copper brought about by diffusion.

5.5 Thermal Fatigue

5.5.1 Introduction. The phenomenon of a decrease in bond strength, and the inferred decrease in thermal conductivity with thermal cycling, is the most serious problem associated with the Ti-Mo-Cu sputtered layer system on BeO. Both titanium diffusion leading to a copper intermetallic formation, and the

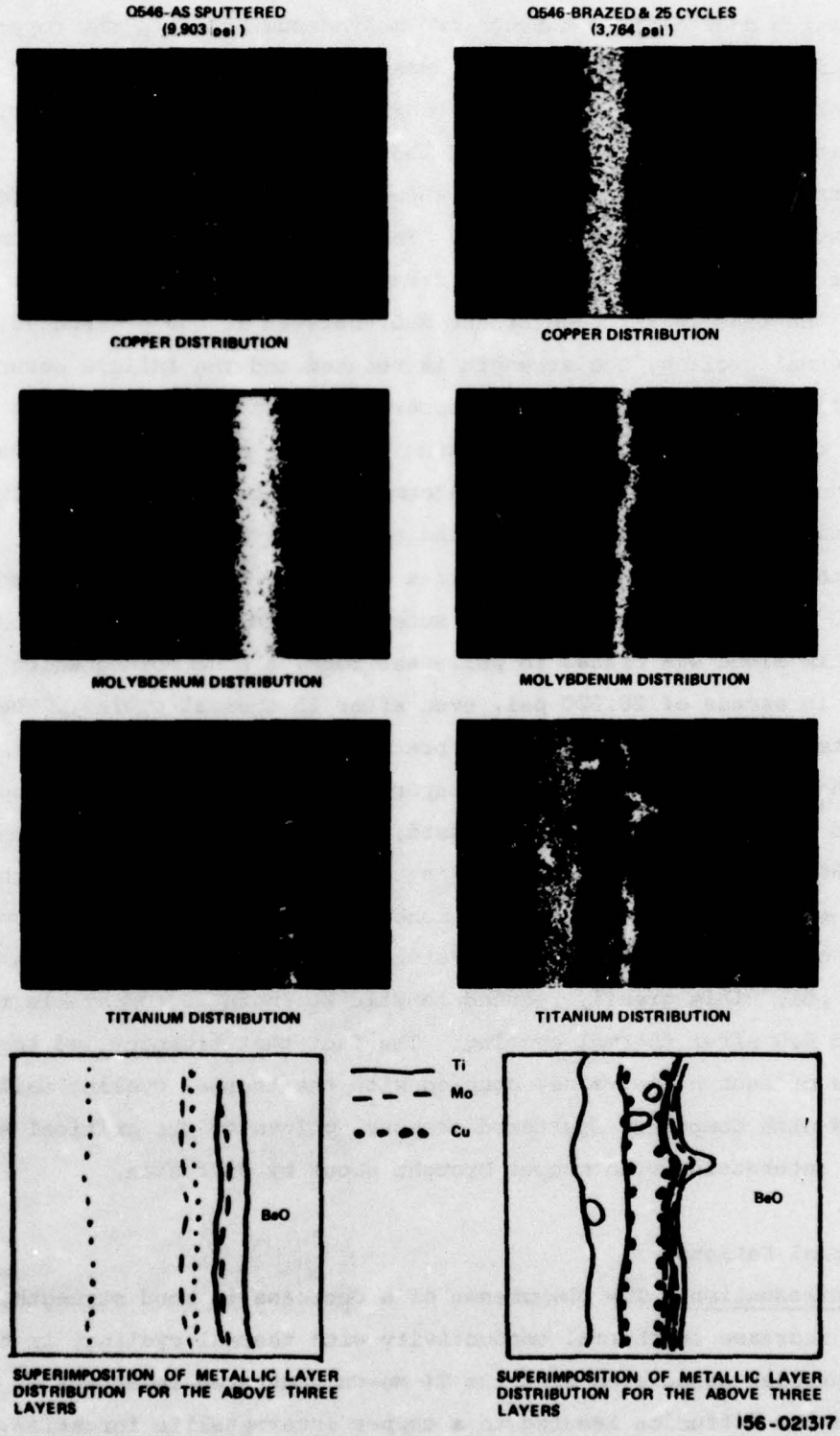

Figure 27. Electron Microprobe Comparison of Sputtered Film Morphology Showing Titanium Diffusion After Thermal Excursions.

a) DIRECT VIEW OF Q509 NO. 1 COUPON AFTER TENSILE FAILURE TEST - NOTE CERAMIC FRACTURE AT POINTS OF CONTACT BY PULL TEST ROD. TENSILE STRESS: 12,430 psi X 10

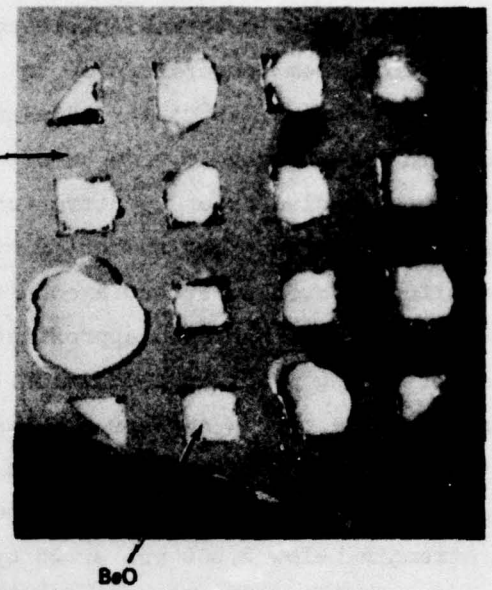

b) DIRECT VIEW OF COUPON Q513 NO. 11, AFTER TENSILE FAILURE. SOME CERAMIC FRACTURE AND SOME COPPER STILL AT POINTS OF CONTACT. TENSILE STRESS: 2626 psi X 10

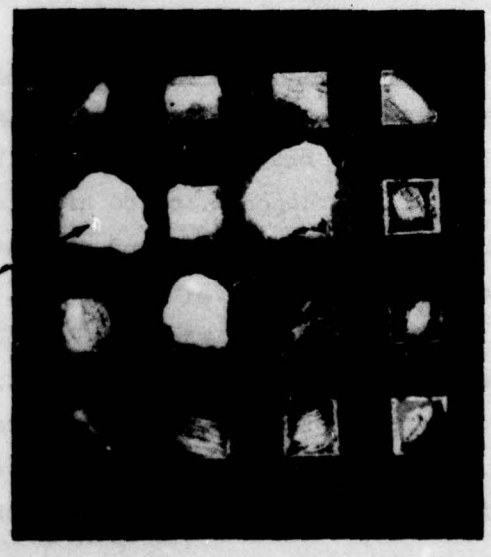

156-021318

Figure 28. Failure Modes With and Without Thermal Cycling.

thermal stresses associated with the different layers, compound to markedly influence bond deterioration. As a single factor, the intermetallic is the more severe problem, but the effect of thermal strain as an accelerator of diffusion accentuates the main problem.

For this work, a thermal cycle consisted of heating a coupon in wet hydrogen from room temperature up to 500°C for 10 minutes, and then cooling to room temperature (25°C) for 15 minutes. This simulates environmental conditions in tube usage, ie, one on-off cycle of the tube at full power. Some samples were cycled prior to diffusion brazing. Others were brazed and then cycled for the prescribed number of cycles before pull testing. The standard or baseline sputtering schedule consisted of depositing 1,500 Å of titanium, 5,000 Å of molybdenum, and approximately 9 μm of copper with no time delay after air firing prior to deposition. The experimental variables and the associated sample coupon numbers are listed in table 7. Table 8 is a summary of the thermal cycling effect on tensile stress. All failure stresses represent three datum points unless otherwise noted. When thermal cycling had reduced bond strength below 2,000 psi or 25 cycles were concluded, no further cycling tests were performed. This was considered to be sufficient to determine the trend and what effect the sputtering process variable had on bonding.

5.5.2 Cycling at 500°C without Brazing. Table 9 is a summary of tensile failure stresses for a standard sputtered coupon with associated thermal cycles prior to brazing. No drastic bond strength reduction is evidenced with cycling of the coupon prior to high temperature (1,015°C) brazing. Any minor reduction of the ultimate bond strength may be associated with the thermally induced stresses between the metallic and ceramic interfaces and is not due to titanium diffusion or intermetallic formation. Failure occurred by ceramic fracture and not a breakdown of the sputtered films. The low variation in failure stress as expressed by the standard deviation is indicative of the low-level influence of cycling alone and suggests the noncritical nature of storing sputtered coupons under ambient conditions.

5.5.3 Hygroscopic Effect on Thermal Cycling. Thermal cycling revealed that the hygroscopic effects of BeO led to an overall deterioration of bond strength (figure 29). For substrates held for more than 1 day after firing

Table 7. Summary of Experimental Variables in the Sputtering Process.

Coupon Number	Experimental Variable
Q509	No delay after air firing and sputtering (Denoted standard sputtering schedule)
Q513	1-day delay after air firing and sputtering
Q518	3-day delay after air firing and sputtering
Q515	7-day delay after air firing and sputtering
Q516	14-day delay after air firing and sputtering
Q519	No air firing
Q520	No titanium
Q523	Poor onset vacuum
Q525	2 times titanium thickness (3000 Å)
Q527	One-half molybdenum thickness (2500 Å)
Q530	No molybdenum
Q531	2 times molybdenum thickness (10,000 Å)
Q546	Standard sputtering and 600°C preheat under vacuum
Q533	Duplicate Q546 with interim cooling
Q534	Sputter etch
Q535	Bias sputter titanium
Q536	Standard sputtering
Q537	Done with Q536 - Equivalent to Q536
Q538	Higher power titanium (1.2 kW vs 1.0 kW standard)
Q540	Copper only

Table 8. Summary of Thermal Cycling Effect on Tensile Strength of Sputtered Film Bonds.

Coupon Number	Tensile Strength - Average of Three Samples (psi)							
	No Cycles		5 Cycles		15 Cycles		25 Cycles	
	X	σ	X	σ	X	σ	X	σ
Q509	11,699	579	-----	-----	-----	-----	-----	-----
Q513	9,757	1,058	7,503	2,327	4,117	1,538	2,418	959
Q518	4,015	809	1,961	1,489	1,829	1,043	-----	-----
Q515	7,027	1,551	3,270	2,589	562	682	-----	-----
Q516	5,152	1,279	3,471	597	2,057	2,315	-----	-----
Q519	6,705	2,078	3,176	1,952	2,147	1,040	1,648	971
Q520	1,987	473	1,934	1,677	471	683	0	0
Q523	4,832	2,614	5,735	1,570	3,829	318	-----	-----
Q525	8,578	871	7,163	2,189	3,320	1,110	5,215	1,374
Q527	6,107	1,272	3,277	494	1,986	860	-----	-----
Q530	5,189	2,220	3,159	790	1,329	1,179	-----	-----
Q531	4,418	1,289	5,058	1,186	1,659	770	-----	-----
Q546	9,424	961	6,640	3,116	3,372	922	4,718	529
Q533	10,196	1,394	8,117	1,553	5,621	1,529	8,065	1,806
Q534	8,705	1,364	6,666	2,541	3,843	274	4,026	317
Q535	1,477	1,138	-----	-----	-----	-----	-----	-----
Q536	9,438	1,745	7,712	1,805	8,025	3,735	4,679	945
Q537	9,817	2,367	-----	-----	-----	-----	6,195	513
Q538	8,601	894	7,842	2,253	4,822	424	-----	-----
Q540	1,359	1,298	-----	-----	-----	-----	-----	-----

Table 9. Thermal Cycling Effect on Sputtered Coupon (Q509) Before Brazing to Rods for Tensile Testing.

Number of Cycles	Tensile Failure Stress (psi) X	σ	Number of Datum Points
None	11,699	579	5
10	10,208	730	3
100	8,882	733	4

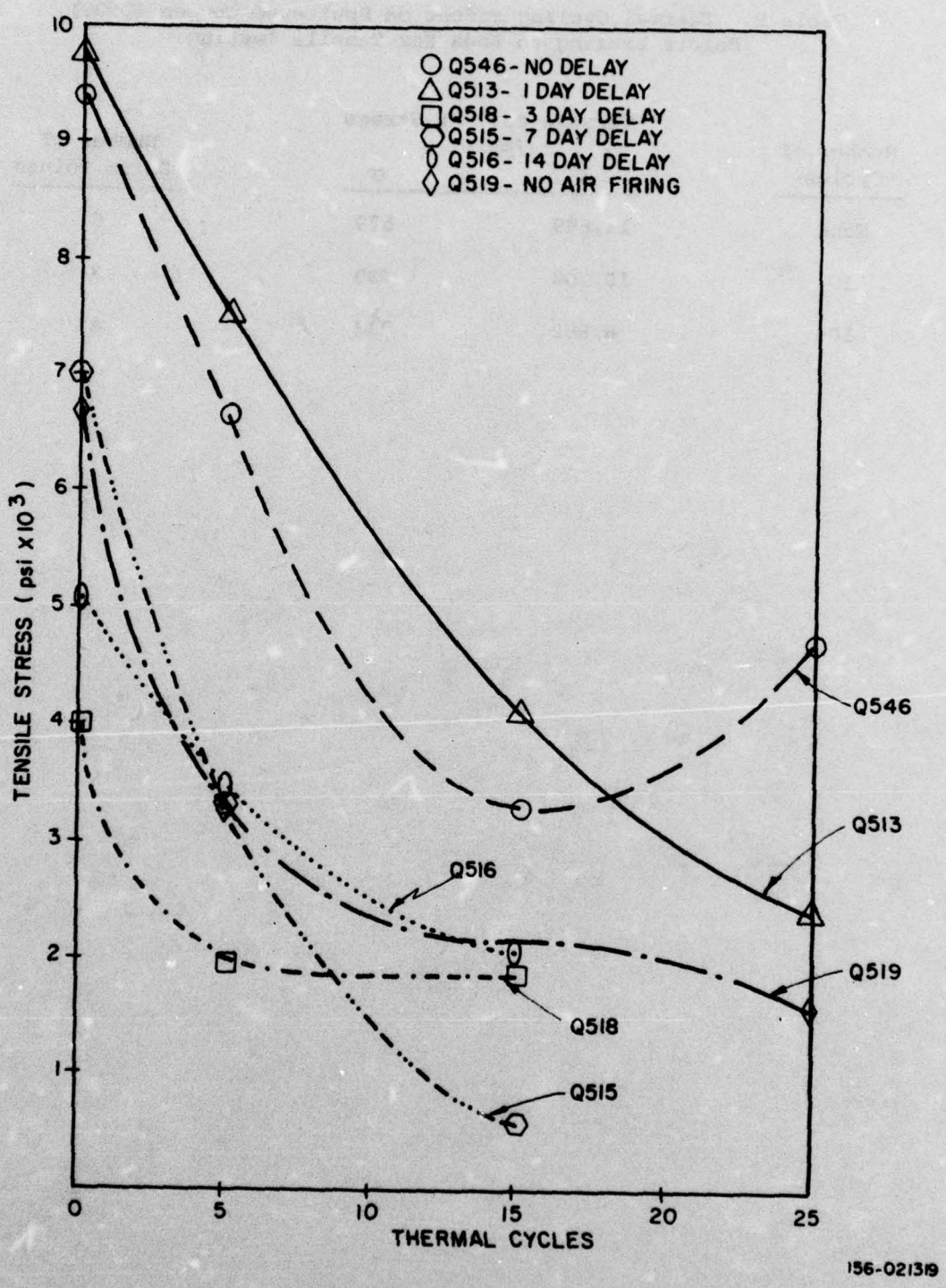

Figure 29. Deterioration of Bond Strength With Thermal Cycling for Samples With Moisture Entrapment.

before sputtering (Q518, Q515, Q516), low initial bond strength resulted and failure below 2,000 psi followed after 15 cycles or less. With only a 1-day delay (Q513), the bond strength loss with cycling approximates that where no delay was allowed (Q546). In the case where no air firing preceded sputtering (Q519), initial bonding was comparable with most samples that had air firing, but after 25 cycles the bond deteriorated to a low level because of residual surface contaminants and moisture. Water on the surface of a virgin coupon is a very important factor, and it must be avoided to produce a useful metallized product because it greatly reduces initial bond strength. Bond deterioration generated by thermal cycling appears to be a cumulative process; therefore, the deterioration to a suboptimum strength level occurs more rapidly because of the lower initial strength level.

5.5.4 The Influence of Molybdenum Thickness on Thermal Cycling. Thermal cycling causes reduced bond strength for various molybdenum layer thicknesses (figure 30). For less than 5,000 Å of molybdenum (Q530-no molybdenum; Q527-2500 Å of molybdenum) the failure mode changes from a ceramic pullout to a metal-ceramic separation. When the molybdenum layer is greater than or equal to 5,000 Å (Q546-5,000 Å of molybdenum, Q531-10,000 Å of molybdenum) failure occurs as ceramic pullout and after cycling results in a copper interface separation. Varying molybdenum thickness does not prevent overall bond weakening with thermal cycling and has very little effect on the overall strength after 15 cycles.

5.5.5 The Influence of Titanium on Thermal Cycling. When titanium is absent, thermal cycling reduces bond strength to zero after 25 cycles (Q520, figure 31), which indicates the important role of titanium in both initial bond improvement and improved thermal cycling resistance (figure 31). With titanium of at least 1,500 Å (Q525, Q546), initial bonding is greatly improved, but decreases with cycling.

An upturn is noted after 15 cycles which does not fit the intermetallic formation hypothesis. Closer inspection of the inflection at 15 cycles for the tensile stress curves (figure 32), with the standard deviation span superimposed, points out that the data points do indeed result in an inflection. The standard deviation spans do not overlap at the minima and the upturn is

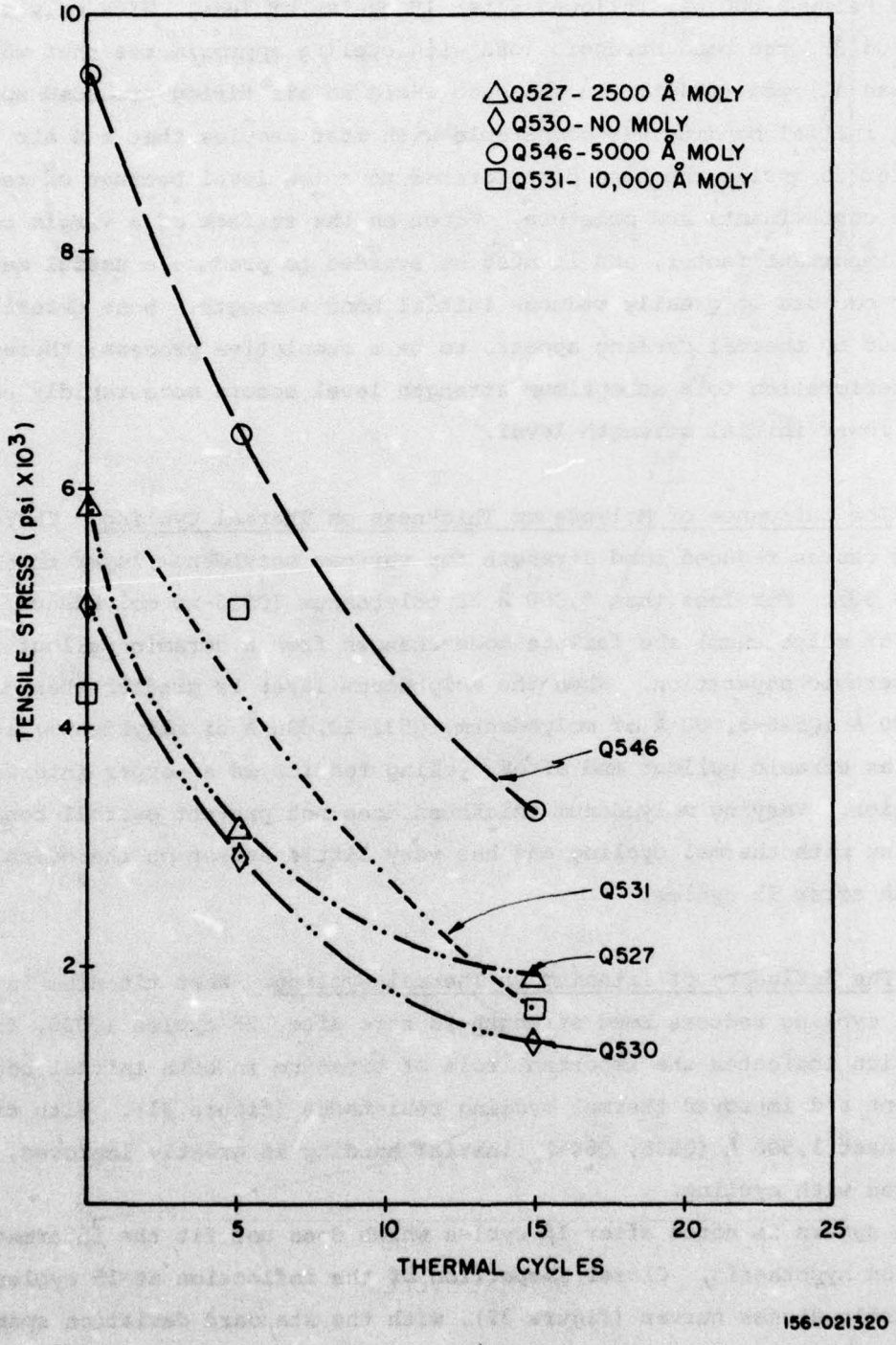

Figure 30. Thermal Cycling Effect on Bond Strength for Varying Molybdenum Thicknesses.

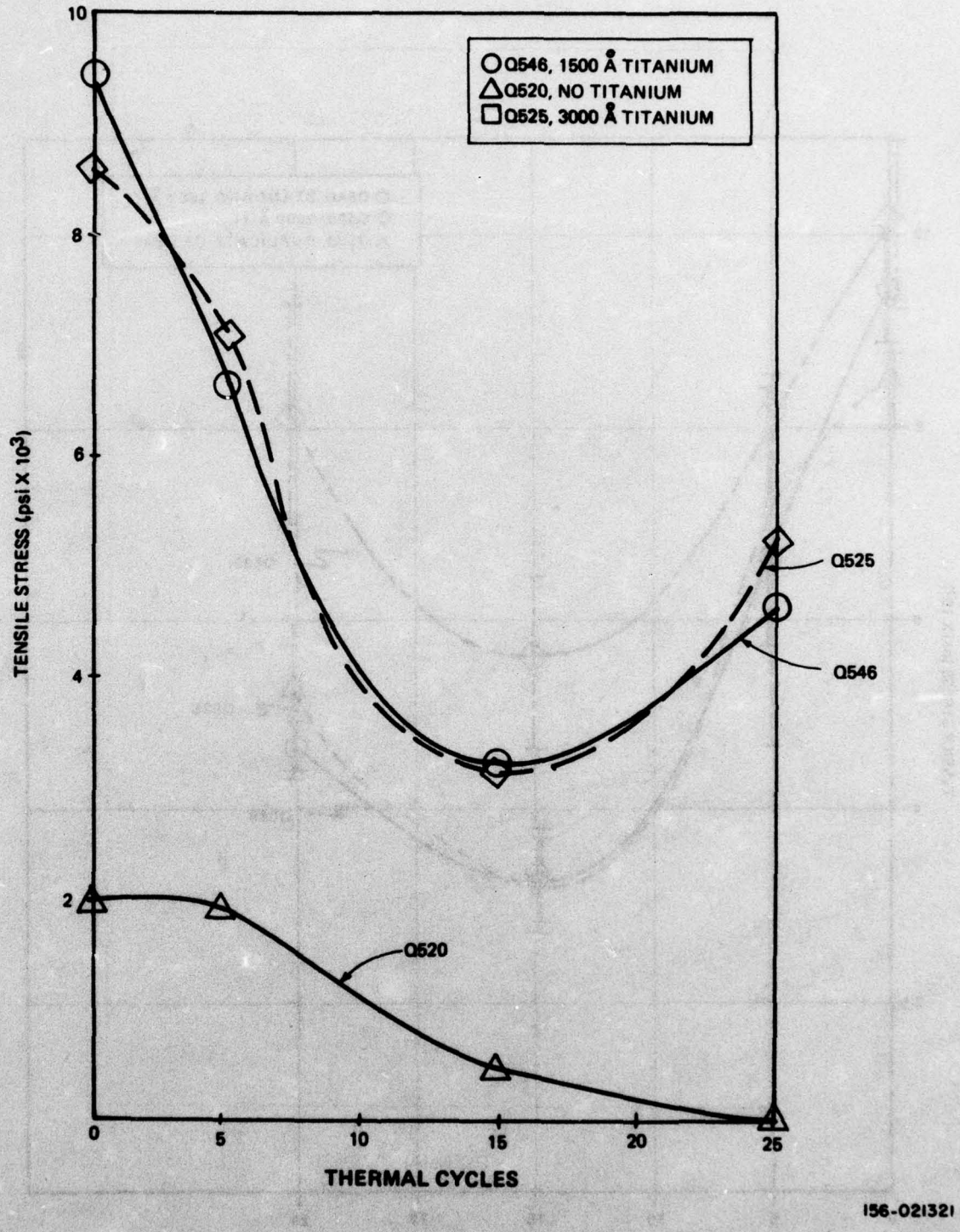

Figure 31. Thermal Cycling Effect on Bond Strength for Varying Titanium Thicknesses.

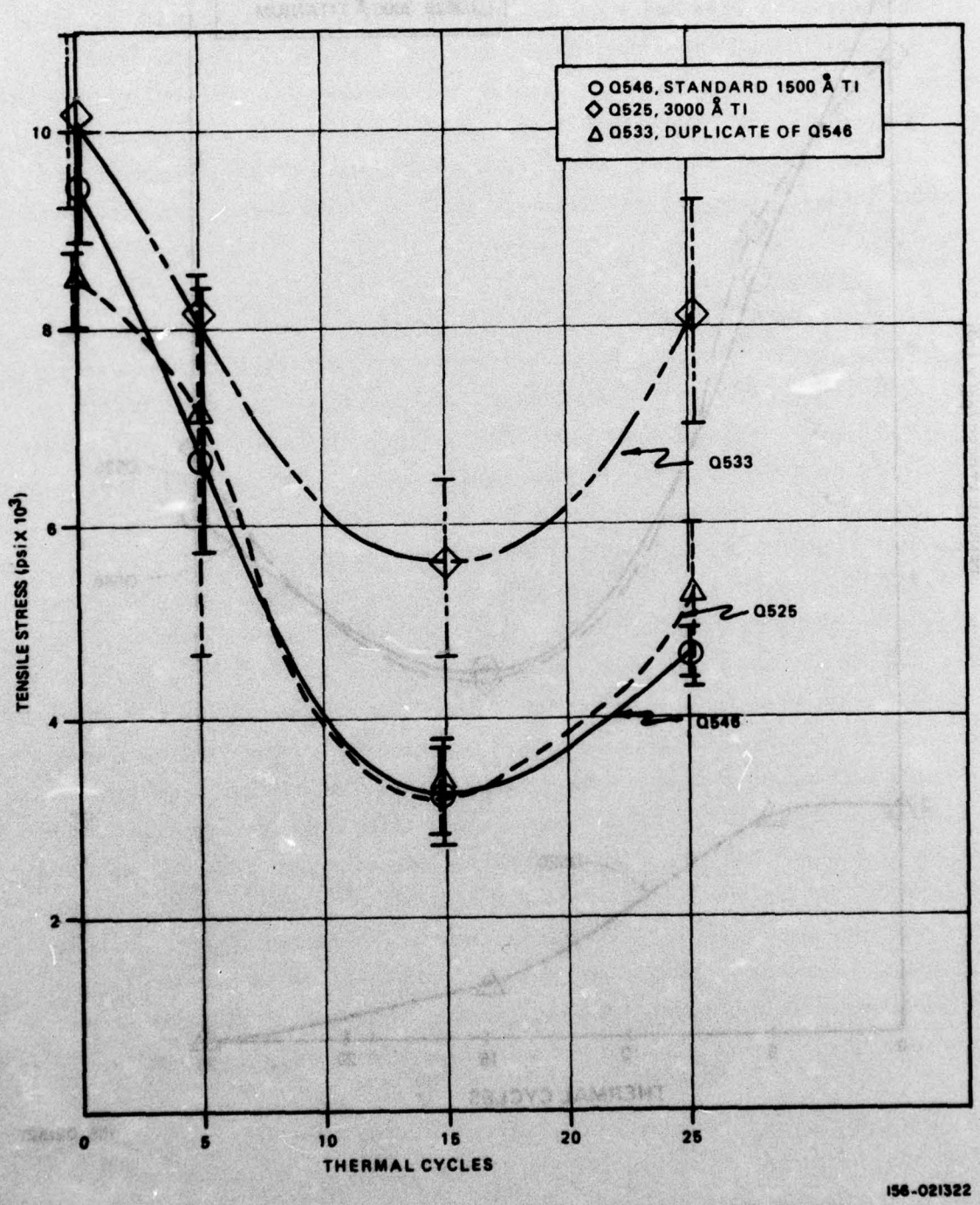

Figure 32. Thermal Cycling Effect on Bond Strength With Minimum Values Plus Standard Deviation Spans.

significant, such that measurement errors should not account for this phenomenon. Also, the trend is observed for three separate coupons sputtered on three different occasions. Q546 and Q533 are identical in their metallic layer thickness, but Q533 had a cooling period during copper deposit. Q525 has similar molybdenum and copper layers but twice the amount of titanium. Only these particular combinations display the decrease followed by an increase of bond strength with thermal cycling. The reason is not understood, but it will be studied in more detail in the next phase of the investigation. Of special interest is the question: does the increasing trend continue, and, if so, why?

5.5.6 Process Alteration Effects on Thermal Cycling. Sputter etching (Q534), which produces copper contamination onto the coupon surface from the underlying copper pallet, does not appear to affect the bonding behavior with thermal cycling (figure 33). The trend follows very closely the results of a coupon which did not have sputter etching (Q546) but did have the same layer thicknesses. The conclusion is that the titanium accounts for the minimal bond strength characteristic observed with thermal cycling.

One variable which does markedly affect the inverted behavior with optimum titanium and molybdenum layer thicknesses is the vacuum achieved prior to sputtering. Coupon Q523 represents a coupon that was sputtered with only a 10^{-4} torr vacuum as opposed to a vacuum of 10^{-5} torr or better for the other coupons (Q533, Q534, and Q546). Initial bond strength is one-half of those where onset vacuum was better. With cycling, a rise in strength results. This must be attributed to some titanium interaction with the beryllia or the reduction of surface contaminants by interstitial diffusion through the sputtered layers. In any event, the initial bond strength value is of relatively low proportions, making initial vacuum an important variable for attaining strong bonds. A measured point for sputtered copper alone is included (Q540) to show the absolutely low bond strength that occurs without titanium (comparison with Q530, figure 31, where titanium and copper were deposited).

5.5.7 Generalizations. The overall conclusions are that air firing increases the initial bond strength attainable and that delay prior to sputtering markedly affects the decrease in strength with cycling, acting as an accelerating

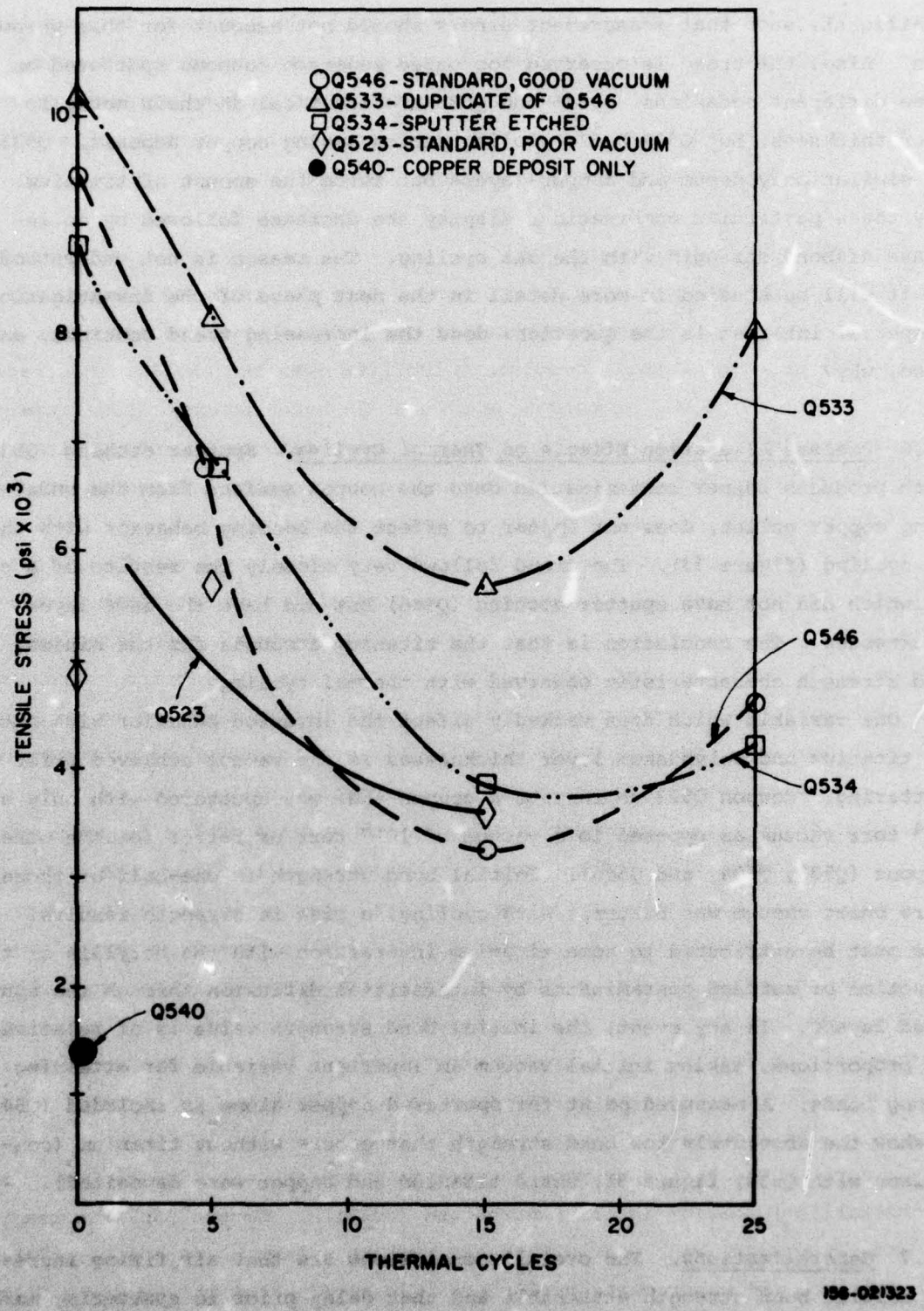

Figure 33. Thermal Cycling Effect on Bond Strength for Standard Sputtered Layer Thicknesses With Different Initial Conditions.

factor. Molybdenum thickness on either side of 5,000 Å reduces fatigue life. Given a molybdenum thickness of 5,000 Å, titanium is necessary to improve bonding and the effect is to produce a minimal trend in bond strength given air firing and good initial vacuum. Sputter etching has no noticeable effect on thermal cycling bond strength behavior.

5.6 Titanium Diffusion Model

As a solid state reaction, diffusion of titanium into and through molybdenum will proceed in a simple substitutional process where no compounds form (figure 34) because of their complete solubility over the whole concentration range. Diffusion should proceed to a typical S-shaped concentration gradient over distance with time. Once the titanium front reaches the copper it would be expected to proceed until an intermetallic composition is reached at about 20 weight percent (25 atomic percent) titanium (figure 35). Once this occurs, any further influx of titanium would result in further compound formations until the whole series of four separate intermetallics as set forth in the equilibrium phase diagram are lined up at the copper-molybdenum interface (figure 36A). This assumes appropriate time for true equilibrium. Also, once established, these intermetallics would be difficult to dissolve to produce diffusion further into the copper, and the various layers would always remain intact. However, what is observed is not as theoretically expected. The intermetallic or high concentration of titanium appears at the copper surface along the diffusion braze to the copper rods as shown in figure 36B. The only explanation for this behavior is that titanium, upon entering copper, diffuses along the grain boundaries at a faster rate than it enters from the molybdenum. It colonizes along the largest grain boundary - sputtered copper to solid copper interface braze, where, based on diffusion rates and energy constraints, nucleation and compound growth occur. Once a compound forms it does not diffuse in the same manner as atomic titanium and is therefore trapped at this location.

A series of experiments were devised to study the titanium diffusion and intermetallic formation in this unexpected location. Coupon Q537 was used; it was sputtered along with Q536, which had cycling stress measurements. Table 10 summarizes the experiments performed. Figure 37 shows the separate film spatial relationships, as revealed by the electron microprobe, in the as-

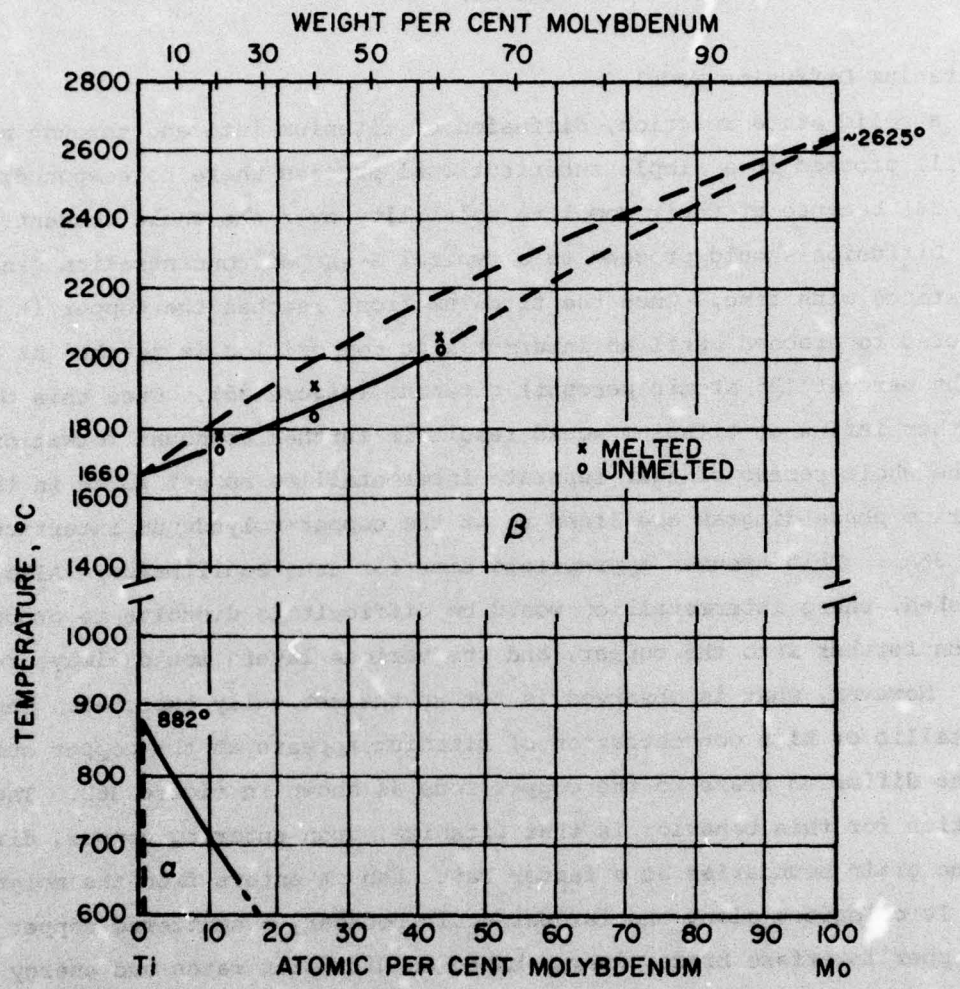

156-021324

Figure 34. Titanium-Molybdenum Binary Equilibrium Phase Diagram.[15]

[15] Hansen, M., Constitution of Binary Alloys, McGraw-Hill, 1958, p 977.

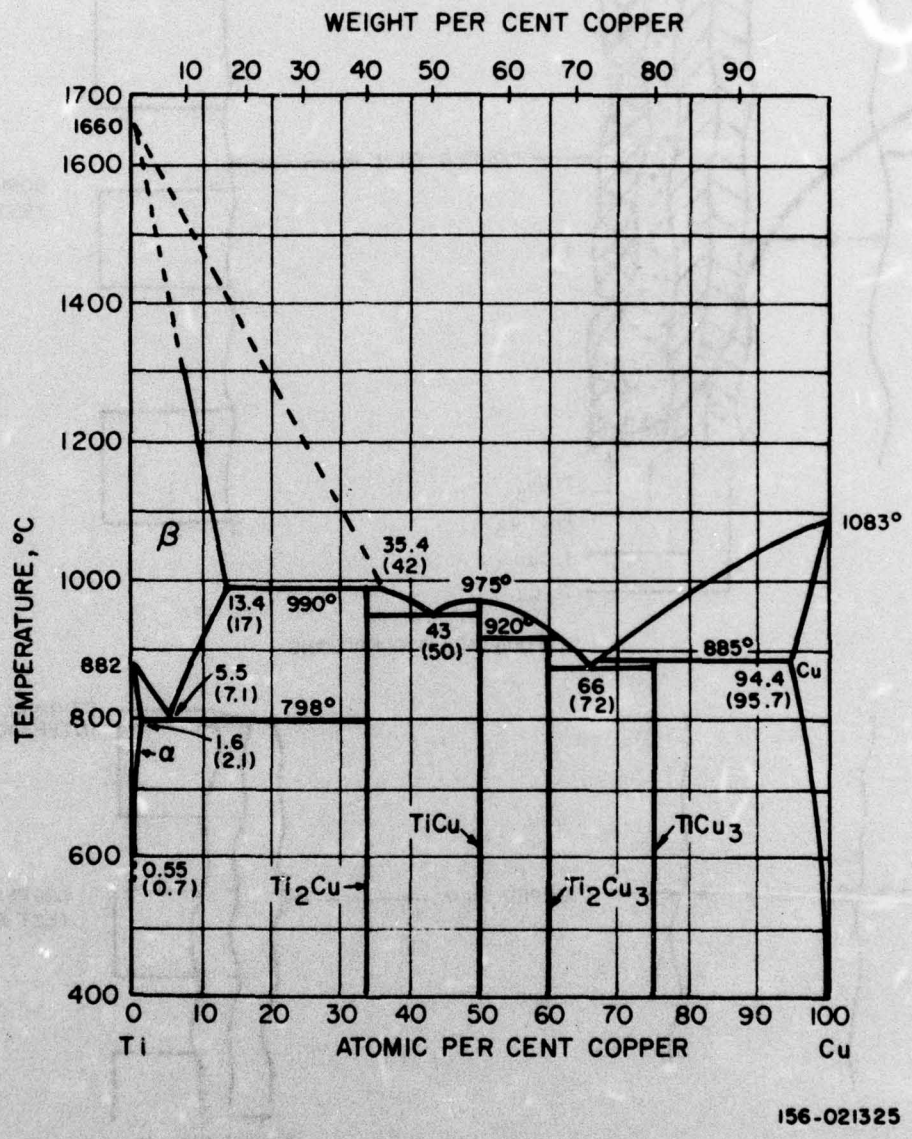

Figure 35. Titanium-Copper Binary Equilibrium Phase Diagram.[16]

[16] Ibid, p. 643.

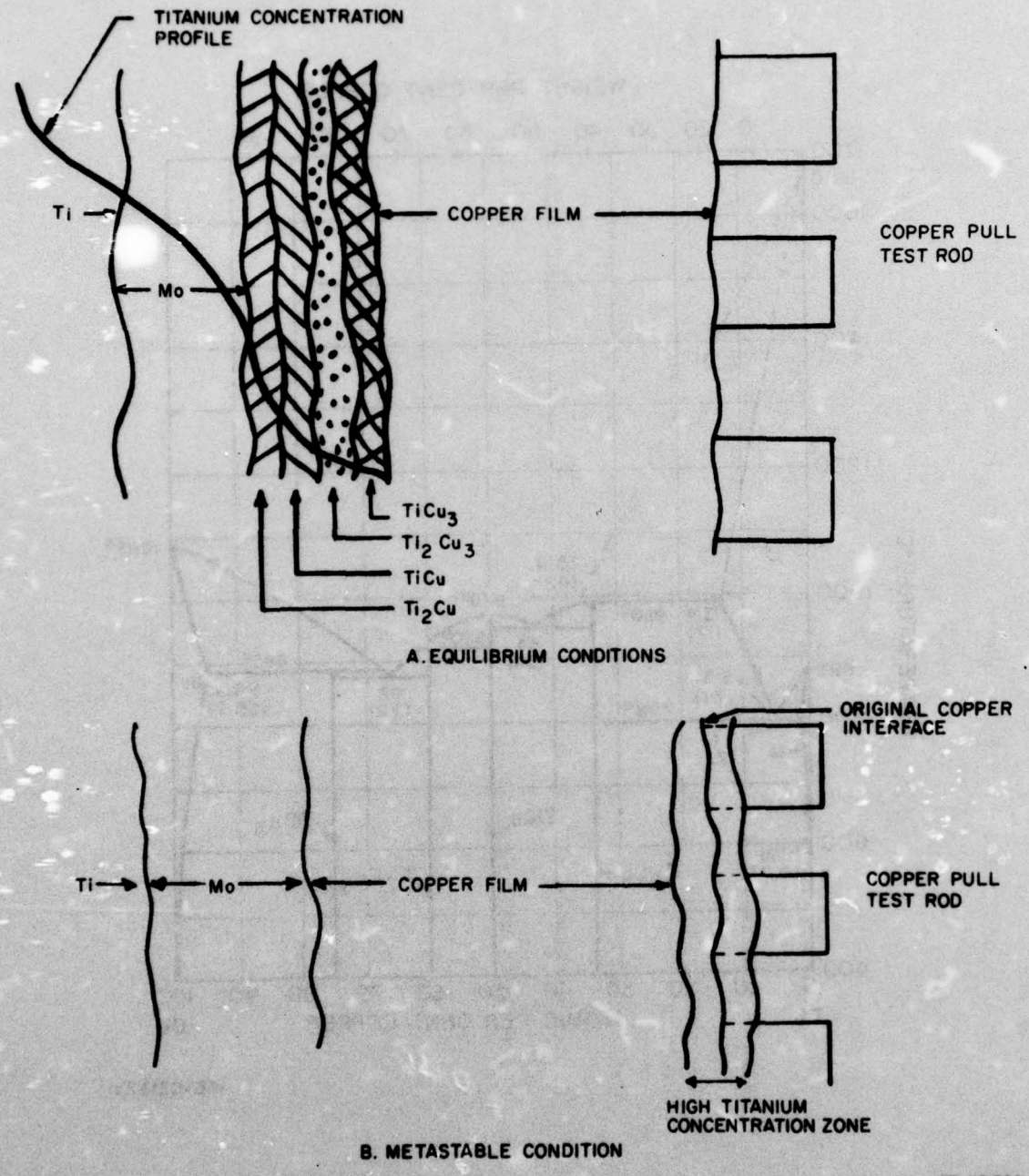

Figure 36. Titanium Diffusion Schematic for the Ti-Mo-Cu Sputtered Layer System.

Table 10. Diffusion Experiments on Sections of Coupon Q537.

Chip No.	Variable	Results
0	As sputtered	Baseline - Ti next to BeO
8	50 thermal cycles on chip only	No Ti diffusion
1	Brazed with rods	Ti-Cu intermetallic formed
11	50 thermal cycles without rods and braze temperature with rods	Ti-Cu intermetallic formed
13	Braze temperature without rods - no cycles	Ti-Cu intermetallic formed
5	Brazed with rods plus 25 cycles	Ti-Cu intermetallic formed
12	Brazed without rods plus 25 cycles	Ti-Cu intermetallic formed

sputtered state. The layers are discrete and continuous, lying next to each other just as they were deposited. Figure 38A shows the titanium morphology after 50 thermal cycles at 500°C without brazed rods. No titanium has diffused into the molybdenum or the copper, signifying that this temperature is insufficient to activate titanium diffusion into molybdenum. Brazing temperature in excess of 1,000°C activates titanium diffusion. Whether the coupon experiences thermal cycling prior to the high temperature excursion or whether copper rods are attached during brazing does not alter the large amount of titanium that colonizes at the free surface of the copper (figure 38B, C, D). Thermal cycling after brazing does not appear to increase the amount of titanium that appears at the copper surface (figure 39), but it is known that bond strength in this region falls off with thermal cycling.

The effect of the rods was expected to alter titanium diffusion because of the additional amount of strain energy introduced with the thermal expansion of the copper rods. At 1,000°C there appears to be sufficient thermal energy to induce titanium to diffuse into and through the molybdenum. Once it enters the copper, the migration occurs so fast that it moves forward along the copper grain boundaries, depleting any entering titanium as fast as it appears. The grain boundary migration proceeds into the copper until the exposed surface of the copper is reached. Once there, buildup occurs because this large grain boundary inhibits further movement, and the process of surface diffusion becomes predominant. Given sufficient concentration of titanium, intermetallic compounds form by nucleation and growth, because of the low energy required for this to occur at the very favorable nucleation sites of the free surface. An intermetallic compound is more stable and it acts to tie up any back diffusion of titanium because the titanium atoms are no longer free to dissolve out of the intermetallic state. The growth process continues until all of the titanium is converted into intermetallic compounds and equilibrium is achieved. This model explains the concentration of titanium at the free surface of the copper and its absence in the copper matrix. Occasionally, dense concentrations of titanium appear within the copper film as islands (figure 38B). Based on the model presented this can be rationalized as a site where compound nucleation occurred because of some imperfection in the copper film, and it behaves exactly like the free surface of the copper once this nucleus has grown to a stable size.

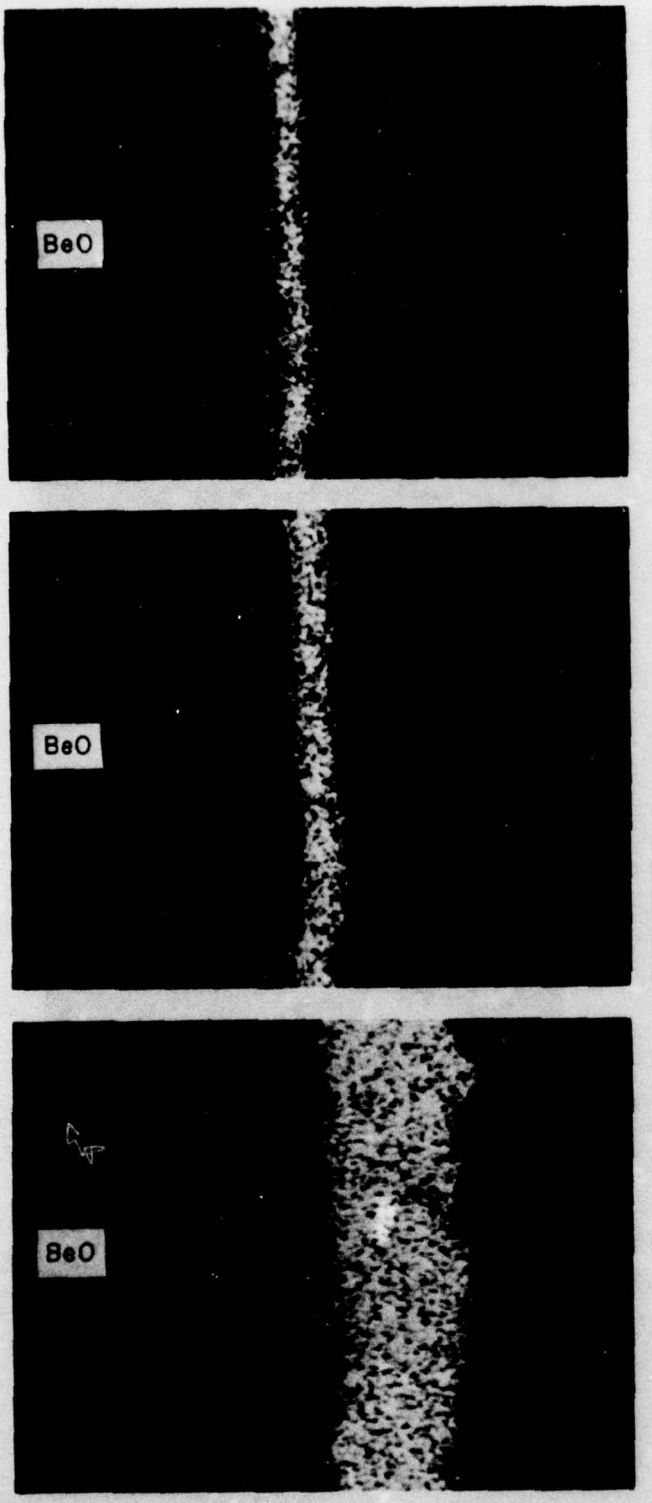

A. TITANIUM LAYER X3000

B. MOLYBDENUM LAYER X3000

C. COPPER LAYER X3000

156-021327

Figure 37. Film Morphology for Q537, As Sputtered, Revealed by the Electron Microprobe.

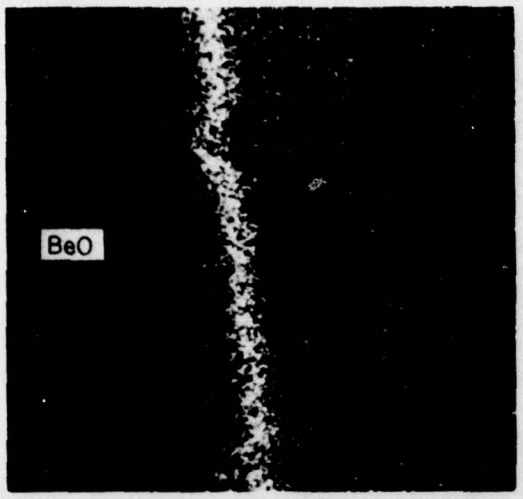

A. 50 THERMAL CYCLES WITHOUT RODS

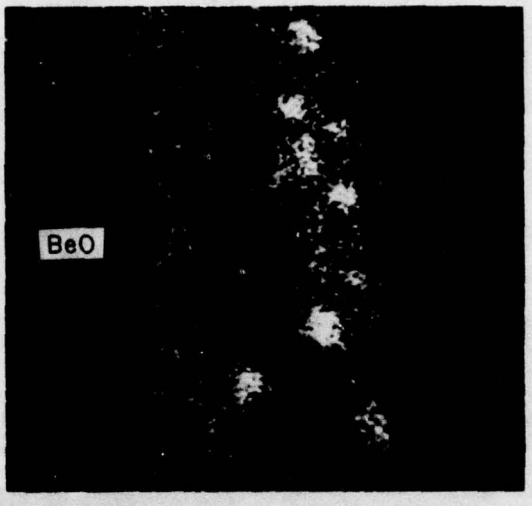

B. BRAZE TEMPERATURE WITH RODS ATTACHED AND NO CYCLES

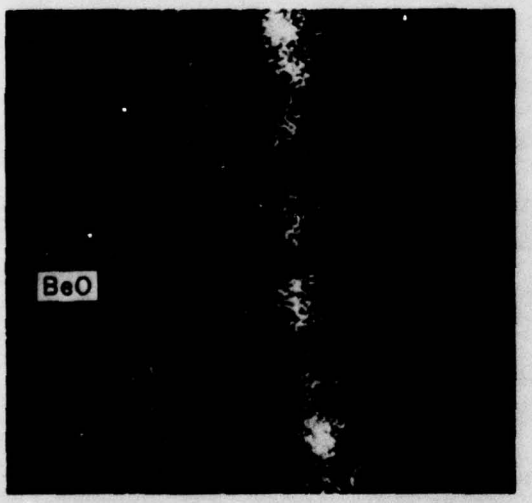

C. 50 THERMAL CYCLES WITHOUT RODS AND BRAZE TEMPERATURE WITH RODS

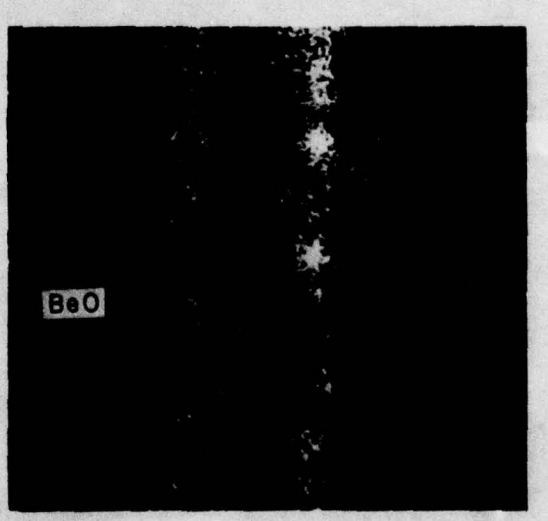

D. BRAZE TEMPERATURE WITHOUT RODS AND NO CYCLES

156-021328

Figure 38. Titanium Spatial Relationships With Thermal Excursions, As Revealed by the Electron Microprobe.

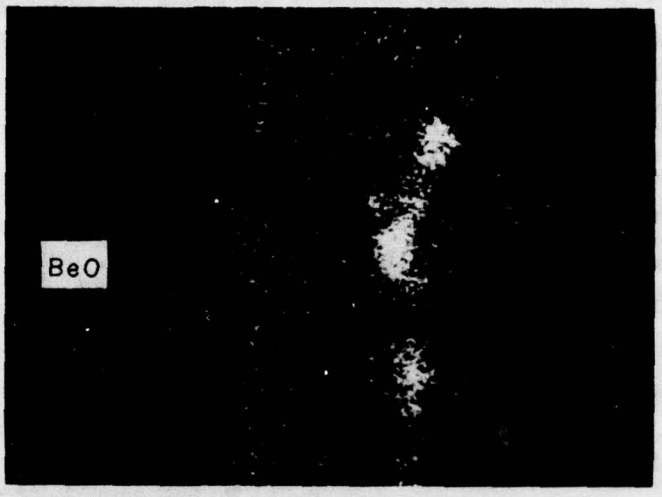

A. BRAZED AT 1015 °C WITH RODS PLUS 25 CYCLES

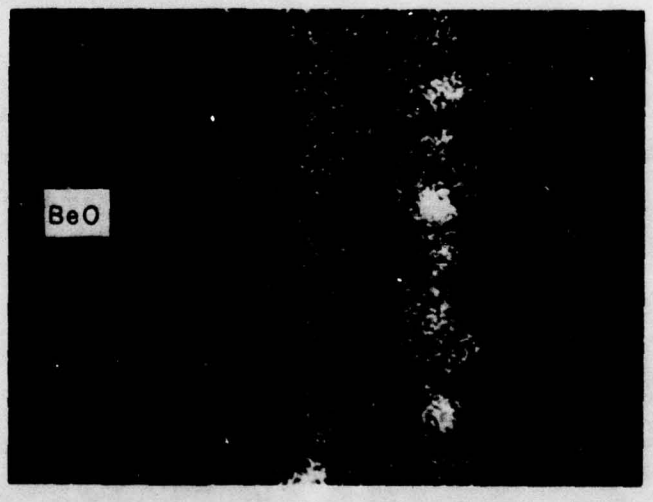

B. BRAZED AT 1015 °C WITHOUT RODS PLUS 25 CYCLES WITHOUT RODS

156-021329

Figure 39. Titanium Spatial Relationships for Cycled Chip After Brazing, As Revealed by the Electron Microprobe.

6. CONCLUSIONS

The removal of hygroscopic moisture from the surface of the BeO substrate by air firing and immediate sputtering is a necessary practice to achieve continuous sputtered films leading to optimum bonding.

Oxygen-free copper alone cannot be sufficiently bonded by sputtering and brazing to BeO at this time to be employed in high power microwave devices.

A molybdenum layer of 5,000 Å is necessary and sufficient to inhibit subsequent copper diffusion at 1,000°C.

The introduction of an active metal such as titanium is one way to achieve maximum tenacity of sputtered metallic films. The mechanism for this bond enhancement is to provide a nonabrupt transition zone from ceramic to metal.

Excessive substrate heating during metal deposition will result in permanent residual stresses which should exhibit themselves in a reduced resistance to thermal fatigue.

Sputter etching does not affect the bond tenacity achieved with the Ti-Mo-Cu metallic system.

Bias sputtering has a negative effect on the bond strength produced, perhaps because of the reduced momentum of atoms arriving at the ceramic surface.

Titanium diffusion through the molybdenum and into the copper, where it reacts to form intermetallics, is the cause of bond deterioration. This effect is triggered by the high temperature excursion required to diffusion braze copper to copper and can proceed to completion at 500°C.

☆ U. S. GOVERNMENT PRINTING OFFICE: 1976 — 757-001/129